Spring 2014

COMPUTER MODELING AND SIMULATION OF IMPLANTABLE MEDICAL DEVICE HEATING DUE TO MRI GRADIENT COIL FIELDS

Bryan David Stem
Purdue University

Recommended Citation

Stem, Bryan David, "COMPUTER MODELING AND SIMULATION OF IMPLANTABLE MEDICAL DEVICE HEATING DUE TO MRI GRADIENT COIL FIELDS" (2014). *Open Access Theses*. 265.
https://docs.lib.purdue.edu/open_access_theses/265

Graduate School ETD Form 9
(Revised 01/14)

PURDUE UNIVERSITY
GRADUATE SCHOOL
Thesis/Dissertation Acceptance

This is to certify that the thesis/dissertation prepared

By Bryan Stem

Entitled
COMPUTER MODELING AND SIMULATION OF IMPLANTABLE MEDICAL DEVICE HEATING DUE TO MRI GRADIENT COIL FIELDS

For the degree of Master of Science in Engineering

Is approved by the final examining committee:

John A. Nyenhuis

Scott D. Sudhoff

Thomas M. Talavage

Jamu K. Alford

To the best of my knowledge and as understood by the student in the *Thesis/Dissertation Agreement. Publication Delay, and Certification/Disclaimer (Graduate School Form 32)*, this thesis/dissertation adheres to the provisions of Purdue University's "Policy on Integrity in Research" and the use of copyrighted material.

Approved by Major Professor(s): John A. Nyenhuis

Approved by: Dale Harris 4/22/2014

Head of the Department Graduate Program Date

COMPUTER MODELING AND SIMULATION OF IMPLANTABLE MEDICAL DEVICE HEATING DUE TO MRI GRADIENT COIL FIELDS

A Thesis

Submitted to the Faculty

of

Purdue University

by

Bryan Stem

In Partial Fulfillment of the

Requirements for the Degree

of

Master of Science in Engineering

May 2014

Purdue University

West Lafayette, Indiana

To my mother and father,

who ignited the spark of learning in my life,

protected it from the wind so it could survive

and provided it fuel to grow.

To my loving wife Jessica,

who makes sure that I don’t burn myself or anyone else with that spark.

ACKNOWLEDGEMENTS

The author would like to thank his advisor John Nyenhuis for the expertise, encouragement, and patience needed to complete this work. The author would also like to thank all of his co-workers at Medtronic who supplied the resources and time to make this possible. It is a pleasure and privilege to be a part of a team dedicated to continuous learning through innovation and quality. In particular John Welter, Len Gramse, and Jacob Chatterton all passed along knowledge and skills that were essential to this thesis. Finally the author would like to thank Jamu Alford who provided not only expertise and guidance but daily encouragement and support.

TABLE OF CONTENTS

LIST OF TABLES

LIST OF FIGURES

Figure Page

Appendix Figure

LIST OF ABBREVIATIONS

ASTM	American Society for Testing and Materials
CAE	Computer-Aided Engineering
CT	Computer Tomography
DBS	Deep Brain Stimulation
DUT	Device Under Test
INS	Implantable Neurostimulator
IR	Infrared
ISO	International Organization for Standardization
MRI	Magnetic Resonance Imaging
PAA	Polyacrylic Acid
RF	Radiofrequency
RMS	Root Mean Square
SAR	Specific Absorption Rate
SCS	Spinal Cord Stimulation
T	Tesla, unit of magnetic strength

ABSTRACT

Stem, Bryan D. M.S.E., Purdue University, May 2014. Computer Modeling and Simulation of Implantable Medical Device Heating Due to MRI Gradient Coil Fields. Major Professor: John Nyenhuis.

For patients with implantable medical devices, the ability to safely undergo MRI scanning is critical to ensuring the highest standard of care. The gradient coils of an MRI generate kilohertz frequency, time varying magnetic fields. These magnetic fields induce a voltage on the external case of metallic, implantable medical devices through electromagnetic induction. Since the magnetic field generated by a gradient coil is time varying, the induced voltage results in the flow of eddy currents which can cause heating effects. These heating effects have been successfully modeled using ANSYS Maxwell and ANSYS Mechanical software packages.

The multi-physics simulation and solution used ANSYS Maxwell for electromagnetic field simulation and ANSYS Mechanical for the transient thermal simulation while utilizing ANSYS Workbench to integrate the models. To validate the model, simulations and physical testing were completed on a number of samples that varied in size and material. The model was then used to simulate the impact of implant size (both radius and thickness) on MRI gradient induced heating.

These results can be used to support MRI safety assessments and design choices for a range of implantable medical devices. The current regulatory landscape requires extensive safety testing that is often expensive and time consuming. While the complicated question of medical device heating due MRI gradient coil fields remains open, computer simulation is now a proven tool that can provide easier and more thorough analysis for future evaluations.

CHAPTER 1. INTRODUCTION

1.1 Importance of MRI

Magnetic Resonance Imaging (MRI) is the gold standard for soft tissue diagnostic imaging in medicine. In 2011, 32 million MRI scans were performed in the United States (IMV, 2012) which translates to about one MRI scan every second. It also represents a significant growth from the 18 million MRI scans in 2001 (IMV, 2012) and the growing demand for this imaging modality. Relative to other medical imaging modalities, MRI provides higher contrast between various soft tissues within the body. For a range of conditions, including cancer and high-risk patients, MRI has the highest rating for appropriateness according to the American College of Radiology (ACR, 2013).

MRI uses non-ionizing magnetic fields and radio frequency (RF) signals to create anatomical images. When used in lieu of computed tomography (CT), MRI mitigates the significant health risks of the ionizing radiation present in CT scans. Based on the 72 million CT scans conducted in 2007, 27,000 potential cancer incidents were projected (Gonzalez, 2009). For conditions where serial, or repeated, scan assessments are needed the additive ionizing radiation dosages of CT are unsuitable and can be helped by substitution with MRI (Smelka, Armao, Elias, & Huda, 2007).

1.2 MRI Components

MRI scanners consist of three major components with each playing a unique and critical function in generating anatomical images: static magnet, radio frequency coils, and gradient coils. The static magnet in an MRI is a superconducting electromagnet that includes a number of coils surrounded by extremely cold liquid helium (Coyne). When current is passed through the coils, a magnetic field is generated. This field is measured in Tesla (T), where 1 Tesla equals 10,000 gauss, and is typically 1.5T or 3.0T for MRIs used in hospitals for diagnostics. Stronger magnets can also be used, often for research purposes, such as the 21.1T magnet built at the National High Magnet Field Laboratory in Tallahassee, Florida (Coyne).

From an imaging perspective, the static magnet aligns the protons in the hydrogen atoms within a person to produce a bulk magnetization that is required for imaging to take place. MRI relies on the fact that the body is made up mostly of water that contains hydrogen atoms that react to the magnetic forces inside a scanner (Coyne). This bulk magnetization is aligned with the direction of the static magnetic field (Clare, 2006). Even though the protons are aligned with the static magnet, they are not all pointed in the same direction with both a high-energy configuration and a low-energy configuration possible. The distribution of high and low energy hydrogen atoms is fairly even with a slightly higher percentage lining up in the low-energy configuration. This small percentage becomes critical for imaging because of the second major component of MRI scanners: radio frequency coils.

Radio frequency coils produce an oscillating magnetic field for a short period of time. This magnetic field is orthogonal to the direction of the static magnetic field and is applied at the Larmor frequency, which is equivalent to the angular frequency of the hydrogen atom's precession (Clare, 2006). The end result is that the extra hydrogen atoms lined up in the low-energy configuration absorb the radiofrequency energy causing them to flip to the high-energy configuration. When the radio frequency coil turns off, the hydrogen releases the absorbed energy which produces a signal that can be detected by the MRI scanner (Coyne). Since different tissues will have varying amounts of water and the signal strength depends on the amount of hydrogen present, radio frequency pulses can differentiate tissue types based on the responses detected.

At this point, we have a bulk magnetization due to the static coil which creates the environment for radiofrequency pulses to allow differentiation of tissue types based on their response which is dependent on water content. The last step is to take this response and produce an image of a particular region, or slice, of anatomy. This is where the gradient coils come in to play. Since the resonance frequency of a hydrogen spin is proportional to the magnetic field that it is experiencing (Hornak), any region that experiences a unique magnetic field can be identified and separated. In an MRI scanner, there are three gradient magnets in the scanner, each of which is oriented in a different dimensional plane (Coyne). By rapidly turning the gradient coils on and off, a unique magnetic field can be created in all three dimensions to produce MRI image slices as a function of location and orientation within the body.

The gradient coils are much smaller and lower strength than the static coil. The gradient coil strength is reported as a magnetic strength (millitesla, mT) that is a function of distance (meters, m). The maximum gradient coil strength of current generation MRI scanners is around 100mT/m (Hornak). Since the gradient coils are rapidly turned on and off, the time-varying magnetic fields they produce are often reported in dB/dt which is measured in Tesla per second. This translates to the rate of change of the magnetic field and will become important when understanding the interactions of MRI fields and implantable medical devices.

1.3 MRI and Implantable Medical Device Safety

For patients with implantable medical devices, the ability to safely undergo MRI scanning is critical to ensuring the highest standard of care. Until recently, patients with active implantable devices, such as pacemakers and neurostimulators, were contraindicated for MRI scans due to the safety risks associated with the interactions between the MRI fields and the device. For these patients, few options existed; all of which were limited. Instead of an MRI, patients with implantable medical devices can undergo a CT, which is not ideal for a range of issues, as discussed in Section 1.1. A second option would be to have the implantable device explanted, receive an MRI, and then have the device re-implanted. In addition to exposing patients to multiple surgeries, this often results in a loss of therapy efficacy due to the difficulties in product placement, such as the percutaneous leads of a neurostimulator. For some patients that require recurring MRIs for a given condition, a cancer patient for example, therapy is simply not possible with a number of implantable devices due to MRI safety concerns.

These limited patient options are the result of a range of interactions between the MRI environment and implantable medical devices. Each of the three main components of an MRI (static magnet, radiofrequency coils, and gradient coils) can interact with an implantable medical device (Nyenhuis, et al., 2005). The static magnet, being a very strong magnet, can cause force and torque on ferromagnetic materials used in implantable medical devices. The radiofrequency coils can cause electrical stimulation and heating, which is the primary hazard for neurostimulation devices (Mohsin, Nyenhuis, & Masood, 2010). The oscillating magnetic field of the radiofrequency coils generates an electrical field within the human body. If an implantable medical device has leads, or wires, they can act as antennas and pick up the electrical field generated by the radiofrequency coils. The result is an electrical current traveling along the length of the device that will dissipate as heat where it is coupled to tissue. For neurostimulators, this coupling occurs at the electrodes, which are next to the area of stimulation that is often sensitive tissue. For spinal cord stimulators, this is inside the epidural space. For deep brain stimulators, this is inside the brain. The combination of critically sensitive tissues and high potential heat makes this interaction the greatest risk for patient safety. The last major component of an MRI, gradient coils, can cause unintended stimulation and heating, which is the focus of this research and explained in depth in the following section.

1.4 Gradient Coil and Implantable Medical Device Interaction

The gradient coils of an MRI generate kilohertz frequency, time varying magnetic fields. These magnetic fields induce a voltage on the device, or case, of an implantable medical device through electromagnetic induction. The induced voltage can be described by the Maxwell-Faraday equation for induction below where E is the electric field produced and B is the magnetic field.

$$\nabla \times \mathbf{E} = -\frac{\partial \mathbf{B}}{\partial t} \tag{1}$$

Since the magnetic field generated by the gradient coils is time varying, the induced voltage results in the flow of eddy currents which can cause heating effects. For an implantable neurostimulator (INS) or pacemaker, heating effects are the result of resistive losses as described by Joule's first law where Q is the generated heat measured in Joules (J), I is the current (ampere, A), R is the resistance of the device, and t is time.

$$Q = I^2 \cdot R \cdot t \tag{2}$$

The magnitude of the heating effect is a function of a number of parameters. One critical parameter is the surface area of the implantable device, with larger surface areas resulting in larger magnitudes of current. Other important parameters include the thickness of the metal and its resistivity. Finally, the heating effect will be a function of location and orientation of the surface of the device with respect to the gradient coils along with the MRI scan parameters including scan time and the strength of the gradient dB/dt.

1.5 Regulatory Landscape

With regards to safety in an MRI environment, implantable medical devices fall into one of three formal categories: MR Safe, MR Conditional, or MR Unsafe (Woods, 2008). MR Safe applies to products that are not magnetic or electrically conductive and also do not interact with a radiofrequency environment. MR Conditional applies to products that can safely undergo an MRI scan under a defined set of parameters (or conditions). These products may or may not be electrically conductive but have proven safety within the range of parameters for which they are labeled MR Conditional. MR Unsafe refers to products that are unsafe for an MR environment or whose safety cannot or has not been definitively proven.

The vast majority of active implantable medical devices fall into the MR Unsafe category and have labeling restrictions preventing scanning in an MRI as controlled by the Food and Drug Administration in the United States (FDA). Recently, pacemakers (Foreman, 2011) and neurostimulators (FDA, 2013), which have historically been labeled MR Unsafe, have successfully gained MR Conditional labeling. In order to gain MR Conditional labeling, the challenge is not only in designing implants that are safe but also proving that the implant is safe in the MR environment, which has been accomplished in clinical studies (Wilkoff, et al., 2011).

As of January 2013, the American Society for Testing and Materials (ASTM) has published test method standards for radio frequency induced heating on or near passive implants (ASTM Standard F2182-11a, 2011), magnetically induced torque on medical devices (ASTM F2213-06, 2011), and magnetically induced displacement force on medical devices (ASTM F2052-06e1, 2006). However, despite being in progress, published ASTM test method standards do not exist for either radio frequency or gradient coil induced heating on or near active implants. The International Organization for Standardization, or ISO, does have a published technical specification for the assessment of safety with MRI and active implantable devices that will eventually become a standard (ISO/TS 10974, 2012).

The lack of a standard increases the resource burden of creating and proving safety for MR Conditional implants. Clinical studies require extensive resources and time and do not always provide a comprehensive analysis. Laboratory experimentation is possible for the range of interactions between MRI scanners and implantable medical devices especially when used in combination with computer simulation. The goal would be to reduce the testing and evidence burden for implantable devices allowing quicker and easier approval for MR Conditional products to reach more patients as soon as possible so they can have access to the standard of care that MRI provides.

CHAPTER 2. BACKGROUND

2.1 Evaluation of Gradient MRI Environments

When evaluating gradient MRI environments in a laboratory setting, it is important to understand the construction and physics underlying a Helmholtz Coil. In general, the gradient coils in an MRI are designed to make linearly changing fields, whereas a Helmholtz coil is designed to make a constant field. Given the size of an implantable medical device relative to the gradient coil, it is reasonable to assume a spatially constant field over the device, which can be generated by a Helmholtz coil. This component is often built independent of the other MRI components to allow for easier evaluation in laboratory settings. Another tool for evaluating gradient MRI environments is computer simulation. ANSYS is the developer of a range of software packages that can be used to simulate electromagnetic fields and environments. These tools are detailed in the following sub-sections as background for the experimental design.

2.1.1 Helmholtz Coil

A Helmholtz coil consists of a pair of circular magnetic coils. The utility of a Helmholtz coil comes from the fact that it can produce a nearly uniform magnetic field within a given region (Sanchez, 2008). For simulation, modeling, and experimentation this provides a framework for producing and analyzing fields that arise from complicated or difficult to reproduce environments, such as the gradient magnetic fields of an MRI.

To create a Helmholtz coil, two coils are placed on opposite sides of an experimental area and an electrical current is passed through the coils. The current is identical and flowing in the same direction for the two coils which are also identical in dimension (radius, *R*), construction and symmetry relative to the experimental area. Figure 2.1 below diagrams a Helmholtz coil with dimensions and parameters labeled.

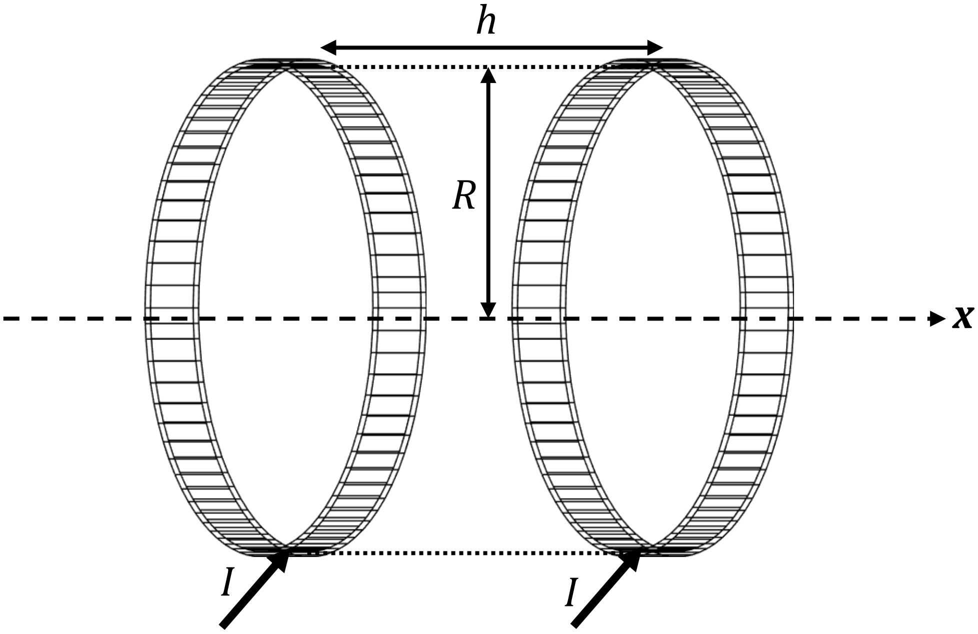

Figure 2.1 Helmholtz Coil Mechanics and Setup

In a construction where the separation distance, *h*, is equal to the radius, *R*, the magnetic field in the *x* direction becomes a uniform, constant field at the center of the coil separation with magnitude (Sanchez, 2008):

$$B_x\left(\frac{h}{2}\right) = \frac{\mu_0\, I}{h} \tag{3}$$

When a specific magnetic field is desired, it can be created by manipulating the current, *I,* in the coils. This provides a setup for both physical laboratory testing and computer simulation validation.

Technically, the gradient coil in the z-axis of an MRI is an anti-Helmholtz coil. An anti-Helmholtz coils has similar construction as a Helmholtz coil except that the electrical currents have opposite directions. This results in axial fields that are in opposite directions (Tipler & Mosca, 2008). As mentioned before, given the size of an implantable medical device relative to the gradient coil, it is reasonable to assume a spatially constant field over the device, which can be generated by a Helmholtz coil.

2.1.2 ANSYS Simulation

A number of software packages exist for the simulation and modeling of electromagnetic fields and field interactions. The software developer ANSYS, Inc., produces two electromagnetic field solvers: HFSS, a full wave solver used for high frequency applications, and Maxwell a quasi-static solver used for low frequency applications. ANSYS Maxwell uses the finite element method to solve static, frequencydomain, and time-varying electromagnetic and electric fields. ANSYS Maxwell can be integrated with ANSYS Mechanical for transient thermal simulations utilizing ANSYS Workbench to sync the models, results, and parameters. When combined, a complete simulation from electromagnetic inputs to thermal response is produced. ANSYS is the preferred CAE (computer-aided engineering) software for this type of problem because of its multi-physics capabilities along with its popularity in both academic and industry settings (Lee, 2012). Popularity provides easier access to training and also examples through a broader community of users.

2.2 Literature Review

The interactions between MRI environments and implantable medical devices have been investigated, studied, and published. Nyenhuis et al. detailed the range of effects for each of the three principal magnetic fields (Nyenhuis, et al., 2005). In this publication, the emphasis for safety is placed on RF-induced heating as shown through the example of neurostimulator leads used for deep brain stimulation (DBS). The potential for heating is highlighted as a patient risk. Additional studies extend upon this work with a thorough evaluation of DBS lead heating as a function of the specific absorption rate (SAR) and safety (Finelli, Nyenhuis, & Gonzalez-Martinez, 2002). In this article, patient safety is explored as a possibility if the MRI operates within a specified range.

The combined effects of the static magnetic field and gradient fields are also explored by Nyenhuis et al. with the conclusion that any interaction is minimal and does not pose a significant risk to the patient (Nyenhuis, et al., 2005) beyond the risk associated with each of the magnets directly. Similarly, heating as a function of gradient induced currents is presented as a theoretical possibility by Schueler, Hammer, and Kucharczyk (Schueler, Hammer, & Kucharczyk, 1999). Following a series of MRI experiments with implantable medical devices, the authors end up concluding that no heating of any of the devices or leads was detected and include a simulation of the induced current density. In the simulation, a worst-case implantable device configuration was modeled as an aluminum spheroid and resulted in a measurable current density. Heating effects due to induced currents in MRI environments have been previously investigated by Buchli, Boesiger, and Meier with no temperature rise measured (Buchli, Boesiger, & Meier, 1988).

Compared to the growing literature on the risks of RF induced heating of implantable devices in an MRI, heating due to gradient coils is substantially less explored. This is mainly due to the significantly higher temperatures, and patient risks, associated with RF induced heating. It is also a function of the difficulty of actual measurements, especially for neurostimulators, that necessitates the need for computer simulations when evaluating induced current (Schueler, Hammer, & Kucharczyk, 1999). Despite the lack of evidence for significant heating due to gradient coils, proof of safety is still required to allow access to MRI with regards to implantable medical device labeling.

Outside of the interaction with implantable medical devices, the effects of gradient coils have been explored with regards to patient safety due to the potential of peripheral nerve and cardiac stimulation (Schaefer, Bourland, & Nyenhuis, 2000). When discussing gradient coil dB/dt limits in the United States Schaefer, Bourland, and Nyenhuis state that there are no numerical limits due to the none-standard location and method of measuring. The maximum switching rate, or dB/dt, of the time-varying magnetic gradient coil was characterized by the Cardiac Rhythm Management Division of St. Jude Medical with research that was presented at the 2011 International Society for Magnetic Resonance in Medicine (ISMRM) conference. According to the research, across a range of 1.5T MRI scanners the maximum dB/dt was 56.5 T/s and occurred in a Siemens Avanto (Butala, Shehada, Constandi, Dianaty, & Jurkowski, 2011). When evaluating the heating of gradient coils on implantable medical devices, the potential dB/dt values for the range of MRI scanners on the market place becomes an important value when translating to patient risk.

CHAPTER 3. EXPERIMENTAL DESIGN

3.1 Evaluation of Modeling Capabilities

In an effort to determine the capability of ANSYS Maxwell to evaluate device heating due to MRI gradient fields, two approaches were used. The first approach was an attempt to re-create the testing environment with a modeled Helmholtz coil. The second approach was generating a uniform H field. While both proved feasible, the uniform H field resulted in easier matching to the test environment and translation to the MRI environments under investigation. The Helmholtz coil approach is discussed as a summary below for context while the uniform H field details the experimental design used for this evaluation.

3.1.1 Helmholtz Coil

With the ANSYS Maxwell software, a Helmholtz coil was created according to the configuration shown in Figure 2.1. Two identical coils were made and an equivalent current was induced in both. When solved, this current successfully generated a magnetic field, shown in Figure 3.1. From the figure, it can be seen that the magnetic field is uniform in the target region at the center of simulation environment. The field does vary near the windings, as expected, but not near the device under test.

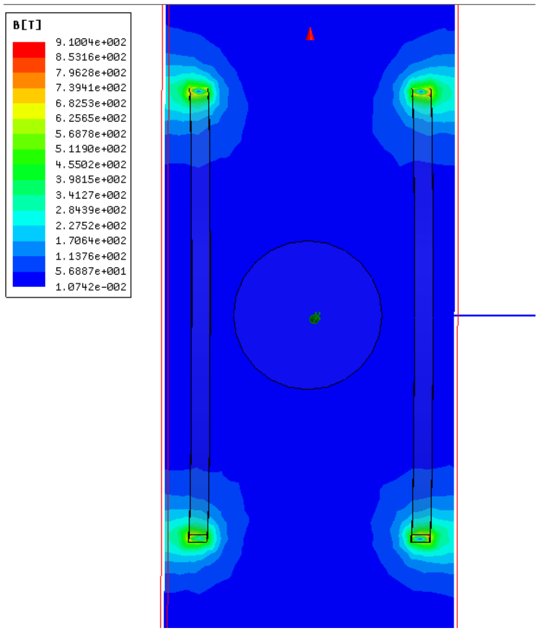

Figure 3.1 Magnetic Field generated by Helmholtz Coil in ANSYS Maxwell

It was also shown that the magnetic field successfully induced an electric field on a device placed in the center of the coils. This is shown in Figure 3.2.

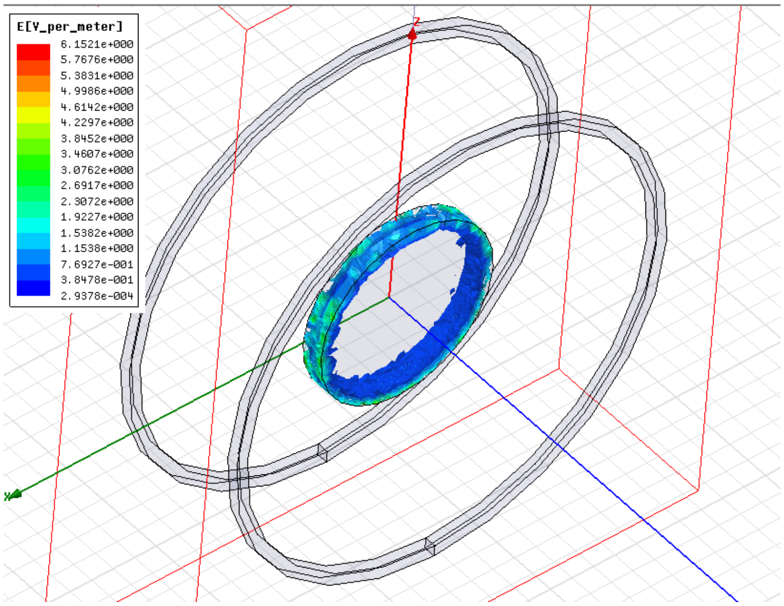

Figure 3.2 Induced Electric Field generated by Helmholtz Coil in ANSYS Maxwell

The ability to re-create the Helmholtz coil with the simulation software is encouraging and potentially useful when designing or testing a gradient coil test station. This would require a more accurate representation of the physical coil elements and geometry. It could also be used to evaluate the impact of subtle physical system variations on the magnetic field. This is beyond the scope of this work but is a potential use of these tools.

3.1.2 Uniform H Field

In ANSYS Maxwell, it is also possible to simulate the time-varying magnetic field of the gradient coil by applying a uniform magnetic field strength, or H Field, to a given region of interest. The H field to be applied can be calculated from a desired time-varying magnetic field and is explained through the equations and steps below. In this thesis, ***B*** is the vector for the magnetic field that has a direction and a time dependent direction. $|\boldsymbol{B}|$ is a vector for the magnetic field that does not contain time dependence. The magnitude of $|\boldsymbol{B}|$ is the peak magnitude of ***B*** and direction is the same as that of $|\boldsymbol{B}|$.

For a given time-varying magnetic field with the following equation where ***B*** is the magnetic field, *f* is the frequency, and *t* is time:

$$\boldsymbol{B} = |\boldsymbol{B}| * \sin(2\pi f t) \tag{4}$$

The rate of change of the magnetic field can be expressed through the following derivative:

$$\left|\frac{d\boldsymbol{B}}{dt}\right| = 2\pi f|\boldsymbol{B}| * \cos(2\pi f t) \tag{5}$$

When solved at time (t) equal to zero, the equation simplifies to:

$$\left|\frac{d\boldsymbol{B}}{dt}\right| = 2 * \pi * f * |\boldsymbol{B}| \tag{6}$$

In the case of an MRI gradient coil, the known dB/dt value can be used to calculate ***B*** as a function of frequency:

$$|\boldsymbol{B}| = \frac{d\boldsymbol{B}}{dt} * \frac{1}{2 * \pi * f} \tag{7}$$

This solution for ***B*** can then be used to calculate the H field through the following equation, assuming there is no magnetic material, where μ_0 is the magnetic constant equal to $4 * \pi * 10^{-7}$ N/A^2.

$$\boldsymbol{H} = \frac{\boldsymbol{B}}{\mu_0} \tag{8}$$

The uniform H field setup is shown in Figure 3.3 below. The left side shows the region where an H field was applied in the vertical, Z-axis, direction, while the right side of the image shows the region where a zero H field was applied.

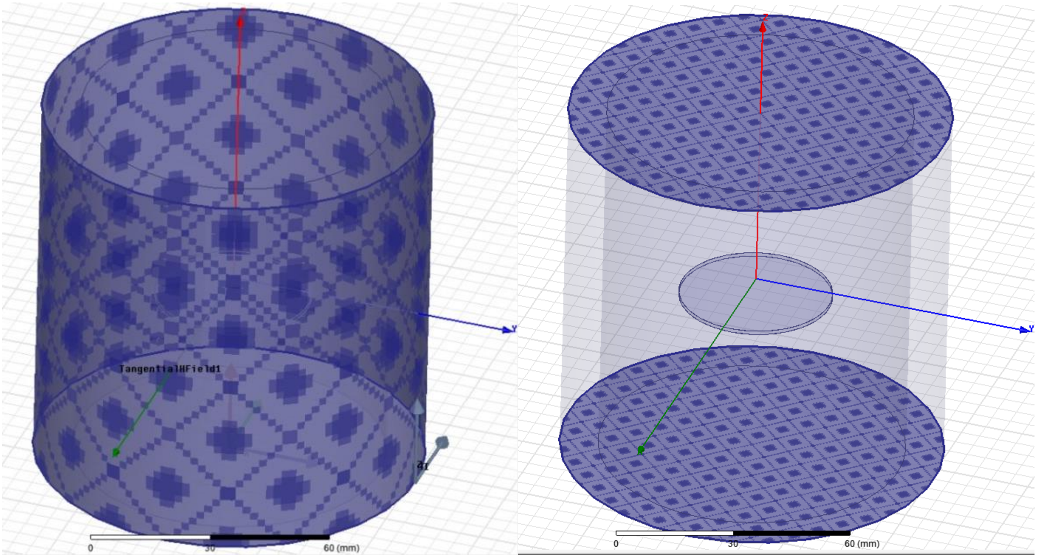

Figure 3.3 Setup of Uniform H Field in ANSYS Maxwell

The disk shown in the center of Figure 3.3 is a test sample, not a field. Additional details for the H field simulation, including specific values, are included in Section 3.2.1.

3.2 Computer Simulation of Device in Gradient MRI Field

The multi-physics simulation and solution used ANSYS Maxwell for electromagnetic field simulation and ANSYS Mechanical for the transient thermal simulation while utilizing ANSYS Workbench to integrate the models. The project schematic from ANSYS Workbench is shown in Figure 3.4. It shows how the model geometry setup in Maxwell was linked to the Transient Thermal evaluation and the Maxwell 3D Solution was an input to the Transient Thermal Setup.

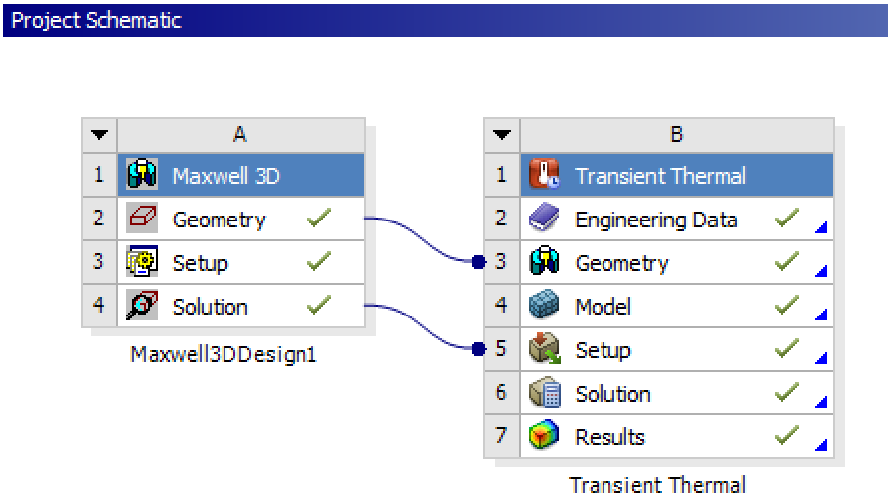

Figure 3.4 Project Schematic for ANSYS Workbench Solution

ANSYS Workbench is used to integrate the models and can also be used to execute the complete simulation. Additional setup details are controlled in each individual software package and explored in the sub-sections below.

3.2.1 ANSYS Maxwell – Magnetic and Electrical Solution

ANSYS Maxwell is used to determine the magnetic and electrical components of the simulation solution. For this series of simulations, the *EddyCurrents* solver of Maxwell 3D was utilized. The project schematic, geometry setup, and geometry visual for the simulations are shown in the following figures. In the project schematic, under Field Overlays, the *NamedExpr* term is a calculated dB/dt value and is illustrated later in Figure 4.5.

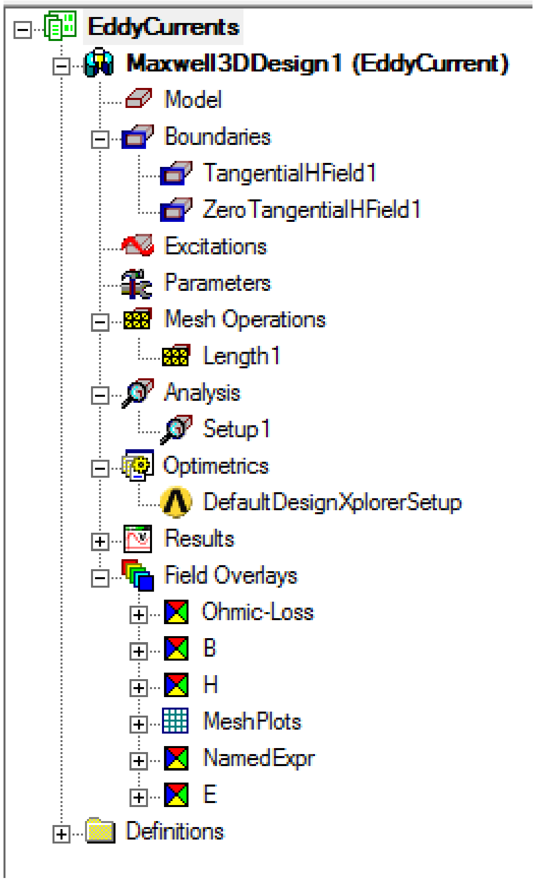

- **EddyCurrents**
  - **Maxwell3DDesign1 (EddyCurrent)**
    - Model
    - Boundaries
      - TangentialHField1
      - ZeroTangentialHField1
    - Excitations
    - Parameters
    - Mesh Operations
      - Length1
    - Analysis
      - Setup1
    - Optimetrics
      - DefaultDesignXplorerSetup
    - Results
    - Field Overlays
      - Ohmic-Loss
      - B
      - H
      - MeshPlots
      - NamedExpr
      - E
  - Definitions

Figure 3.5 Project Schematic for ANSYS Maxwell Setup

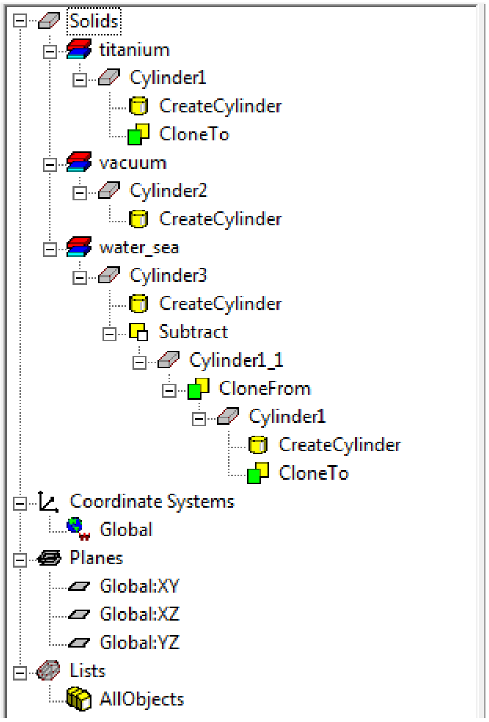

- Solids
  - titanium
    - Cylinder1
      - CreateCylinder
      - CloneTo
  - vacuum
    - Cylinder2
      - CreateCylinder
  - water_sea
    - Cylinder3
      - CreateCylinder
      - Subtract
        - Cylinder1_1
          - CloneFrom
            - Cylinder1
              - CreateCylinder
              - CloneTo
- Coordinate Systems
  - Global
- Planes
  - Global:XY
  - Global:XZ
  - Global:YZ
- Lists
  - AllObjects

Figure 3.6 Geometry for ANSYS Maxwell Setup

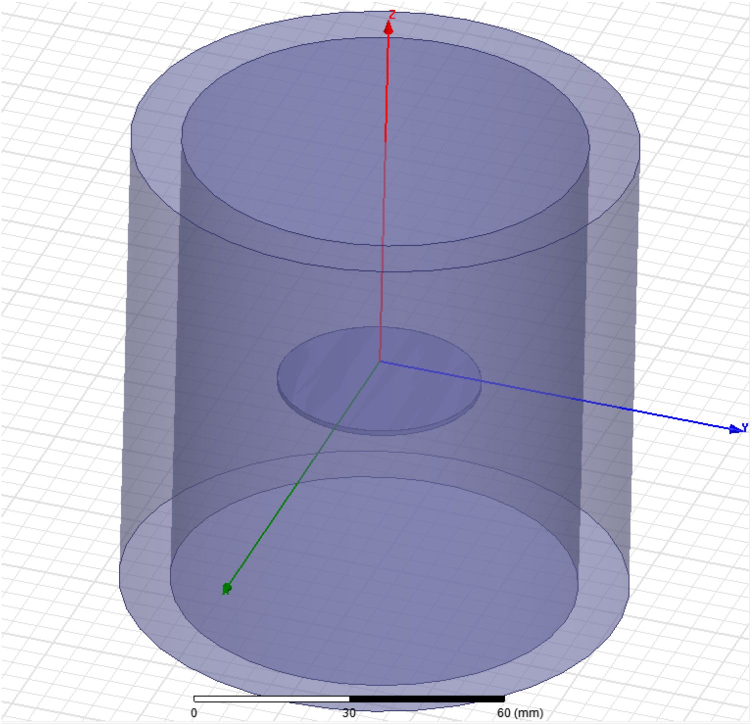

Figure 3.7 Visual Geometry for ANSYS Maxwell Setup

When comparing Figure 3.6 to Figure 3.7, Cylinder 1 is the medical device sample in the center of the visual. Cylinder 2 is the outer-most cylinder in the drawing and is represented by a vacuum. This cylinder provides the geometry for the H field boundaries shown in Figure 3.3. The H field Z component of the cylindrical tangential H field shown on the left of Figure 3.3 is shown in the following equation where f is frequency, and s is the unit for seconds to cancel the time component of frequency.

$$H_z = \frac{20{,}000{,}000}{2\pi f} * \frac{1}{s} \tag{9}$$

The H field Z component was created as a function of frequency to allow a frequency sweep of solutions in future simulations. It is calculated from the equations derived in Section 3.1.2 for a desired dB/dt of 25 T/s at 500Hz.

Cylinder 3 is the middle cylinder and provides the saline environment equivalent to the physical test environment. The geometries of cylinders 2 and 3 are included in the following table.

Table 3.1 Cylinder Geometry Values for Uniform H Field ANSYS Maxwell Simulation

Name	**Cylinder 2**	**Cylinder 3**
Center Position	0cm, 0cm, -5cm	0cm, 0cm, -5cm
Axis	Z	Z
Radius	8.95cm	8.255cm
Height	10cm	10cm

The mesh operation was defined only on the device under test and is length based with a maximum length of the elements being 2mm and the maximum number of elements being 5000. More refined meshes were tried with negligible impact to the final temperature values. The analysis setup was adaptive with a maximum number of passes of 5 with a 1 percent error. The convergence was set as 30% refinement per pass with a minimum number of passes of 4 and minimum converged passes of 1. The solver was completed at an adaptive frequency of 500Hz. The bulk conductivity for each of the simulated device materials is included in Table 3.2 in the following section.

3.2.2 ANSYS Mechanical – Thermal Solution

ANSYS Mechanical is used to solve the thermal component of the simulation. As shown in Figure 3.4, it utilizes the geometry created in ANSYS Maxwell along with the electromagnetic solution. The project schematic setup for the ANSYS Mechanical simulation is shown in Figure 3.8. This schematic does not include convection, which was included when modeling liquid saline but not when modeling the gelled saline, also called polyacrylic acid (PAA). Both scenarios were simulated for each device. The convection coefficient for each simulation was calculated from the maximum simulated ohmic loss value, the temperature rise, and geometry of each sample.

The ANSYS Mechanical Product Version used was: 14.5.7. A transient thermal simulation was conducted with an initial temperature of 22°C. The simulation *Analysis Settings* were setup for a 30 minute scan with a minimum time step of 0.18 seconds and a maximum time step of 20 seconds. The imported load comes from the Maxwell3DSolution as an imported heat generation in units of W/m^3. Given the range of samples tested, the statistics for node and element numbers varied for each simulation. The material properties used for the range of test samples are summarized in Table 3.2.

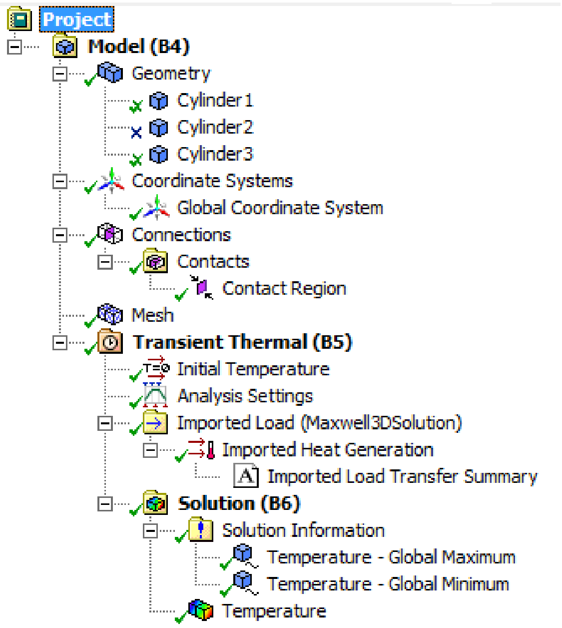

- Project
  - Model (B4)
    - Geometry
      - Cylinder1
      - Cylinder2
      - Cylinder3
    - Coordinate Systems
      - Global Coordinate System
    - Connections
      - Contacts
        - Contact Region
    - Mesh
    - Transient Thermal (B5)
      - Initial Temperature
      - Analysis Settings
      - Imported Load (Maxwell3DSolution)
        - Imported Heat Generation
          - Imported Load Transfer Summary
      - Solution (B6)
        - Solution Information
          - Temperature - Global Maximum
          - Temperature - Global Minimum
        - Temperature

Figure 3.8 Project Schematic for ANSYS Mechanical Setup

Table 3.2 ANSYS Mechanical Material Properties

Material	**Thermal Conductivity (W / m*C)**	**Density (kg / m^3)**	**Specific Heat (J / kg*C)**	**Bulk Conductivity (siemens/m)**	**Relative Magnetic Permeability (μ/μ_0)**
Titanium Grade 1	21	4500	522	1820000	1.00005
Titanium Grade 5	6.7	4430	526.3	561798	1.00005
Stainless Steel	13.8	8055	480	1100000	1.004

3.3 Laboratory Experimentation

In order to fully evaluate implantable device heating due MRI gradient fields, laboratory experimentation was required for both an evaluation of realistic heating profiles and also to validate the computer simulation. This section details the experimental methodology including equipment and procedures.

3.3.1 Test Equipment

Test equipment is detailed in the following table. It is important to note that for the purpose of this testing a full MRI scanner is not required since the evaluation is focused on gradient coil induced heating. Over a small region, the gradient coil field can be approximated by a continuous field. For this reason, a gradient test station that produced a time varying, spatially constant field is acceptable for representative testing of the gradient coils from an MRI scanner.

It is also important to note that two mediums are included for testing. A liquid saline is used for testing with convection and a gelled saline, also called PAA, is used for testing without convection. The gelled saline is more representative of tissue, such as that in the epidural space for spinal cord stimulation, but both mediums are included for testing in order to better analyze the abilities and accuracy of the computer simulation.

Table 3.3 Test Equipment List

Item	**Details / Description**
Gradient Test Station	Resonance Research Inc. Model BFM-180 SPM Used to generate gradient fields that are equivalent to MRI gradients from a device heating perspective. Test station is capable of producing pulsed magnetic fields up to dB/dt of 500 T/s.
Test Fixture	Custom test fixture designed to fit the Gradient Test Station and hold a range of test sample sizes while positioning temperature probes. Shown in Figure 3.9.
Infrared Camera	FLIR T400 Used to capture infrared images of test surfaces in order to evaluate heat distribution and identify maximum heating locations.
Temperature Probes	Luxtron FOT Fiberoptic Thermometers
H-Field Probe	17.9cm diameter, single turn shielded
Oscilloscope	2 channel
Saline (liquid)	De-ionized or distilled water mixed with sodium chloride with a conductivity of 0.47 siemens/meter.
Saline (gelled), PAA	De-ionized or distilled water mixed with sodium chloride (salt) and polyacrylic acid with a conductivity of 0.47 siemens/meter.

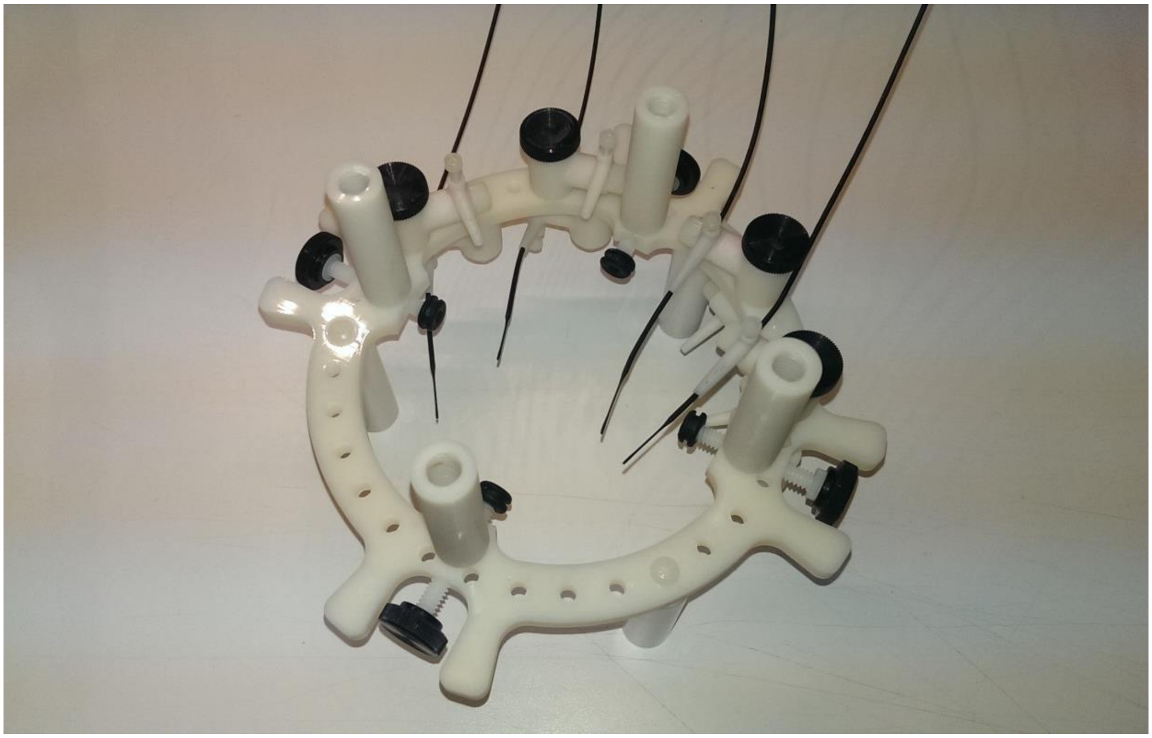

Figure 3.9 Test Fixture with Four Luxtron Probes used with Gradient Test Station

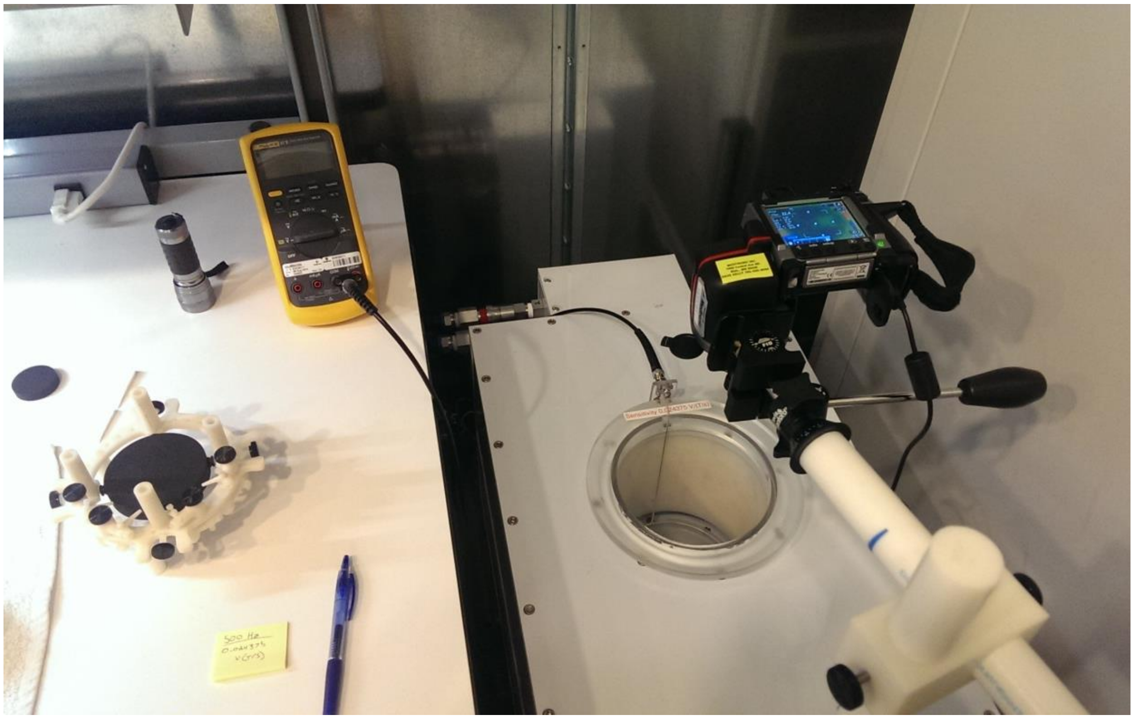

Figure 3.10 Gradient Test Station and Infrared Camera Setup

3.3.2 Test Procedure

The overall procedure consists of two different tests for each sample type. First, the thermal profile of the entire surface is characterized using an infrared camera for each geometry type to be investigated. During this test, the locations of maximum temperature, or "hot spots," are identified. Second, longer scans are run with Luxtron fiberoptic temperature probes on the hot spots to characterize the heating profile continuously over a longer period of time.

3.3.2.1 Thermal Profile with Infrared Camera

Details of the test signal are provided in the table below followed by the test procedure.

Table 3.4 Infrared Test Parameters

Frequency	500 Hz continuous triangle wave B field
Amplitude	25 T/s rms dB/dt
	609 mVrms (as measured in 17.9cm diameter H-field probe)
Duration	10 minutes

1. Place the device under test (DUT) in the test fixture and place the test fixture in the center of the gradient test station with the largest face of the DUT perpendicular to the gradient field, which is the axis of the Helmholtz coil.
2. Fill the test environment with gelled saline (PAA), ensuring that the DUT remains in the center of the setup.

3. Setup the test signal to generate a square wave measured by the H-field probe equivalent to 25 T/s rms by adjusting the waveform generator on the gradient test station, which is producing a continuous triangle wave signal.
4. Place the infrared (IR) camera over the setup and monitor the infrared temperature profile. Make sure that the camera is focused on the DUT and actively monitoring temperature variations.
5. Apply the gradient test signal for 10 minutes and monitor the IR image, saving an image to the memory card every minute. Distortion on the LCD screen of the IR camera due to the gradient environment is normal and will not affect the images saved.

3.3.2.2 Maximum Scan Temperature Testing

Details of the test signal are provided in the table below followed by the test procedure.

Table 3.5 Temperature Probe Test Parameters

Frequency	500 Hz continuous triangle wave B field
Amplitude	25 T/s rms dB/dt
	609 mVrms (as measured in 17.9cm diameter H-field probe)
Duration	30 minutes

1. Place the device under test (DUT) in the test fixture and place fiberoptic temperature probes on the four hottest spots identified in the thermal profile testing, 2 per side.
2. Place the test fixture in the center of the gradient test station with the largest face of the DUT perpendicular to the gradient field, which is the axis of the Helmholtz coil.
3. Fill the test environment with liquid saline ensuring that the DUT remains in the center of the setup.
4. Setup the test signal to generate a square wave measured by the H-field probe equivalent to 25 T/s rms by adjusting the waveform generator on the gradient test station, which is producing a continuous triangle wave signal.
5. Record temperature with the test signal off for 20 seconds to obtain baseline temperature data. The temperature should be recorded at 1 second intervals.
6. While continuing to record temperature, turn on the test signal for 30 minutes.
7. Turn off the test signal and continue to record temperature for 10 minutes to obtain the curvature of the temperature decrease.
8. Repeat steps 1 through 7 replacing the liquid saline in Step 3 with gelled saline (PAA).

3.4 Device Variations

In addition to a range of test samples, a complete matrix of simulations is completed to understand the impact of key variables on device heating. The laboratory test samples along with the expanded simulation samples are detailed in the subsections below.

3.4.1 Laboratory Test Samples

Laboratory test samples along with their dimensions and material details are provided in the following table.

Table 3.6 Laboratory Test Sample List

Sample Name	**Material**	**Diameter (cm)**	**Thickness (cm)**
Large Puck	Titanium, Grade 5	7.62	1.27
Small Puck	Titanium, Grade 1	3.78	0.95
Flat Puck	Titanium, Grade 1	3.78	0.05
Washer	Stainless Steel	7.00	0.30

3.4.2 Simulation Design of Experiments Matrix

Following the successful validation of the accuracy of the computer simulation technique, a design of experiments is completed to understand the impact of both diameter and thickness of devices on gradient induced heating. The following graph and matrix outlines the analysis configurations. These simulations do not have convection terms.

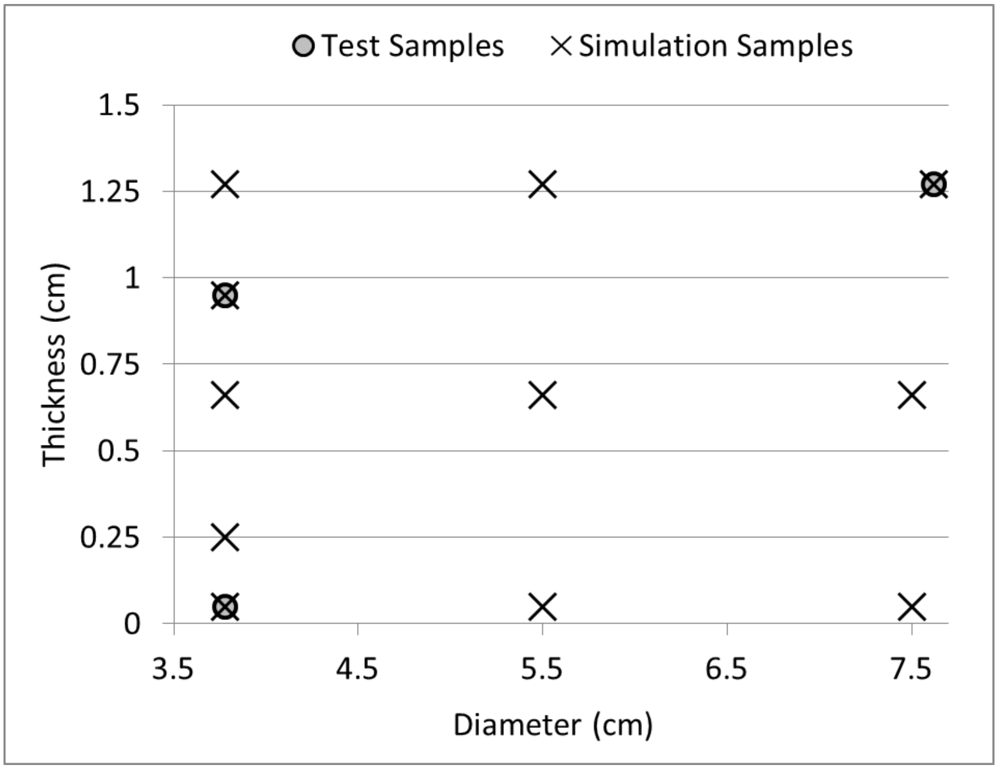

Figure 3.11 Graph of Simulation Test Matrix

Table 3.7 Simulation Matrix Table

Sample	Diameter (cm)	Thickness (cm)	Sample	Diameter (cm)	Thickness (cm)
*1	3.78	0.05	7	5.5	0.66
2	3.78	0.25	8	5.5	1.27
3	3.78	0.66	9	7.5	0.05
*4	3.78	0.95	10	7.5	0.66
5	3.78	1.27	*11	7.5	1.27
6	5.5	0.05			

** Denotes a simulation sample equivalent to a physically tested sample*

CHAPTER 4. RESULTS AND ANALYSIS

4.1 Computer Simulation of Device in Gradient MRI Field

The heating effects due to gradient MRI coils on implantable devices have been modeled using ANSYS Maxwell and ANSYS Mechanical. The simulation results are detailed in the following sub-sections. The first sub-section details the range of data in the ANSYS Maxwell solution. It includes representative graphs from one of the samples for the various fields and values analyzed. The second sub-section includes the thermal solutions from ANSYS Mechanical for the complete list of test samples in Table 3.6.

4.1.1 ANSYS Maxwell – Magnetic and Electrical Solution

The ANSYS Maxwell solution for each sample results in a number of field overlays, as listed in Figure 3.5. This includes the magnetic B field, H field, E (electrical) field, Ohmic-Loss, and dB/dt. For each of these fields, a representative graph is included below from the Thin Puck sample. The complete sets of images were generated for each of the test samples, but are not included here because they show similar patterns.

The following two figures show the magnetic B and H fields. As expected, both fields are relatively uniform throughout the test environment. Minor distortion due to the presence of the medical device can be observed in the color gradients. However, when looking closely at the scale, it is clear that the distortion is minor and the field is effectively uniform.

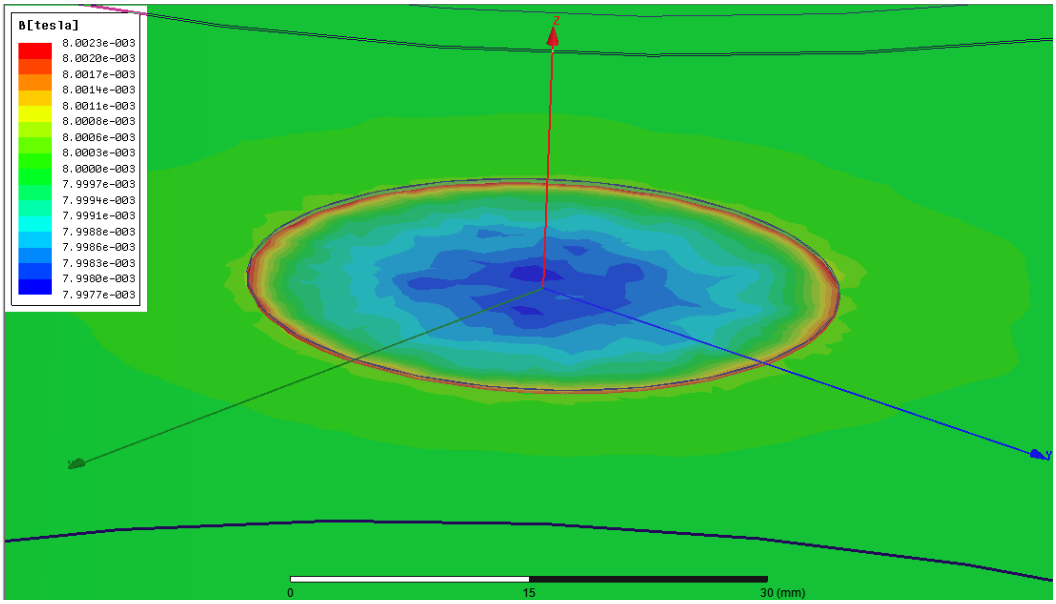

Figure 4.1 ANSYS Maxwell B Field for Thin Puck Sample at Gradient of 25 T/s in Saline

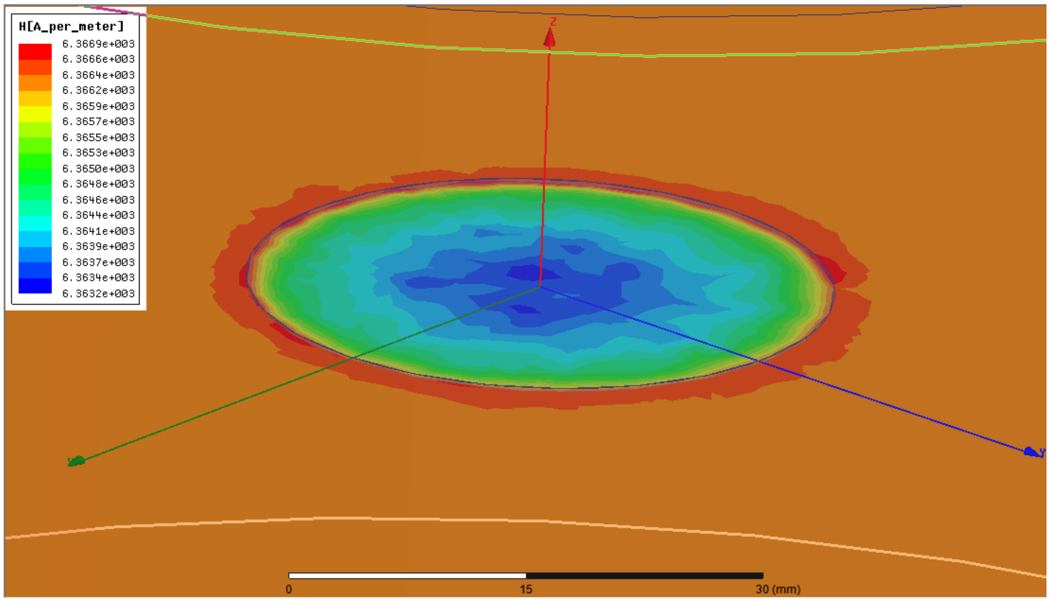

Figure 4.2 ANSYS Maxwell H Field for Thin Puck Sample at Gradient of 25 T/s in Saline

The electrical field, or E field, induced on the sample is shown in the following figure. The electric field does have a range of values with the outside edges of the medical device having a greater field than the center of the device. Since this is the electric field due to the current flow induced on the device, no electric field is displayed in the saline medium surrounding the device.

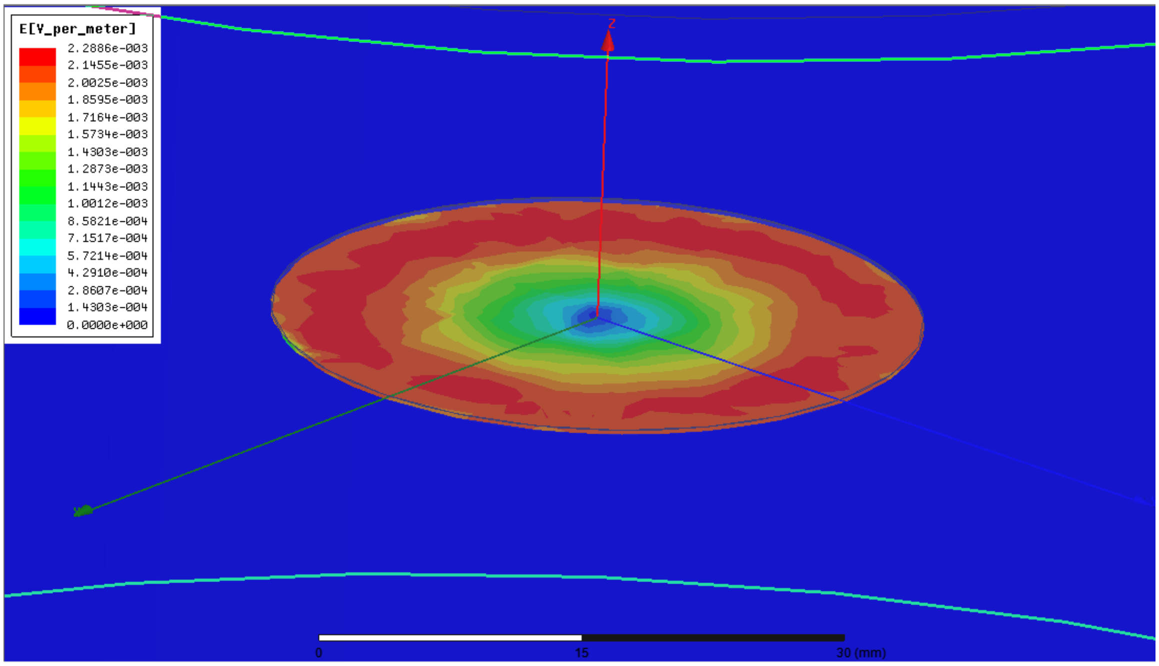

Figure 4.3 ANSYS Maxwell E Field for Thin Puck Sample at Gradient of 25 T/s in Saline

As an effect of the electric field, a visual of the Ohmic Loss is shown in the following figure. It is in units of W/m^3 (watts per meter cubed). As expected, the distribution of the ohmic loss follows the same pattern as the electric field induced on the medical device with larger loss on the outside edges and lower loss in the center of the device.

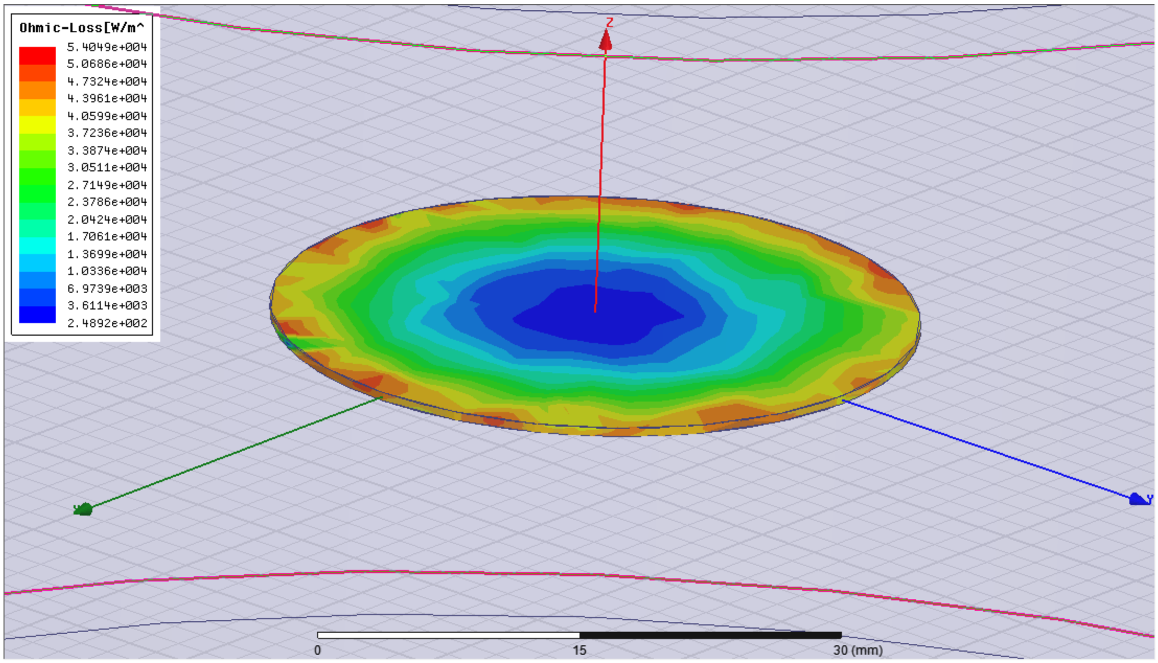

Figure 4.4 ANSYS Maxwell Ohmic Loss for Thin Puck Sample at Gradient of 25 T/s in Saline

The final field overlay is a manually calculated field, dB/dt, calculated from the following equation where f is the solution frequency and $|\boldsymbol{B}|$ is the magnitude of all three components of the magnetic B field:

$$\frac{d\boldsymbol{B}}{dt} = 2 * \pi * f * |\boldsymbol{B}| \tag{10}$$

The derivation of this equation is included in Section 3.1.2.. This equation ensures that the simulated environment is equivalent to the test environment used. An example of the dB/dt field overlay is shown in the following figure.

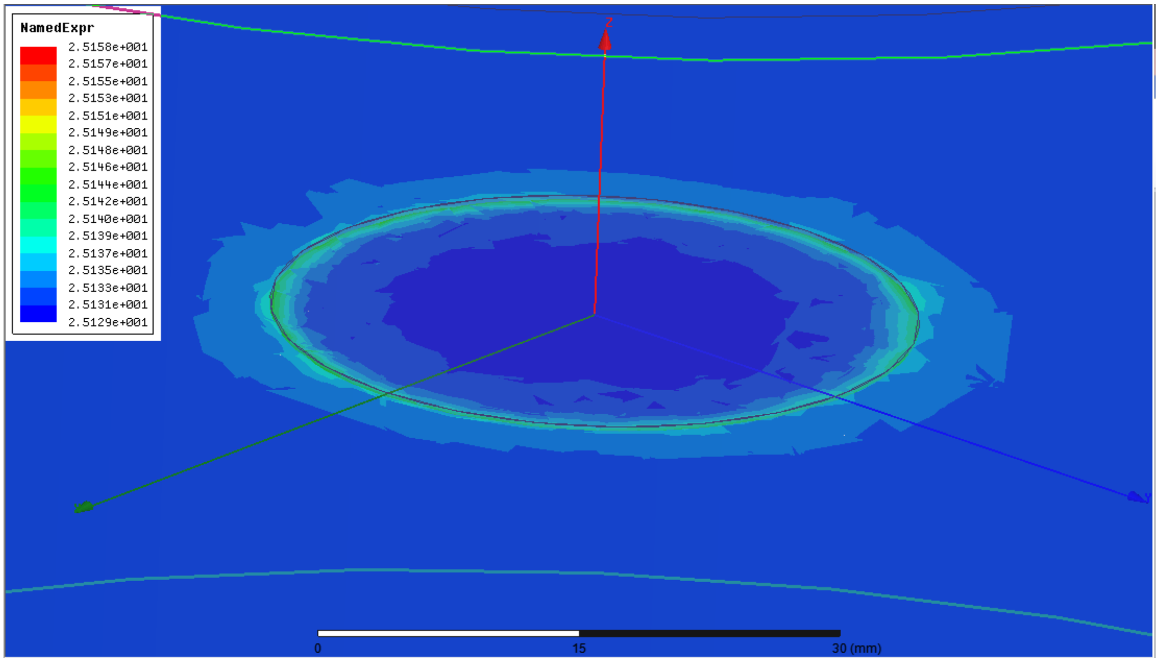

Figure 4.5 ANSYS Maxwell dB/dt for Thin Puck Sample at Gradient of 25 T/s in Saline

From the figure, it can be seen that a uniform dB/dt of 25T/s existed over the entire test environment. Minor distortion is observed due to the implant, but this had a minimal effect on the actual field. The ability to manually calculate and confirm the dB/dt for each simulation ensured that the correct H field input was used in order to match the physical testing environment.

4.1.2 ANSYS Mechanical – Thermal Solution

The complete output data for the set of ANSYS Mechanical simulations is too large to include in its entirety in this report. Graphics of the transient thermal solutions for the four samples both physically tested and modeled without convection are included in Appendix A. These images show the heat distribution across the surface of each of the samples and can be compared to the infrared imaging taken in the physical testing that is also included in the Appendix. The maximum simulated heat rise with convection as a function of scan time for the four test samples is plotted in the following graph.

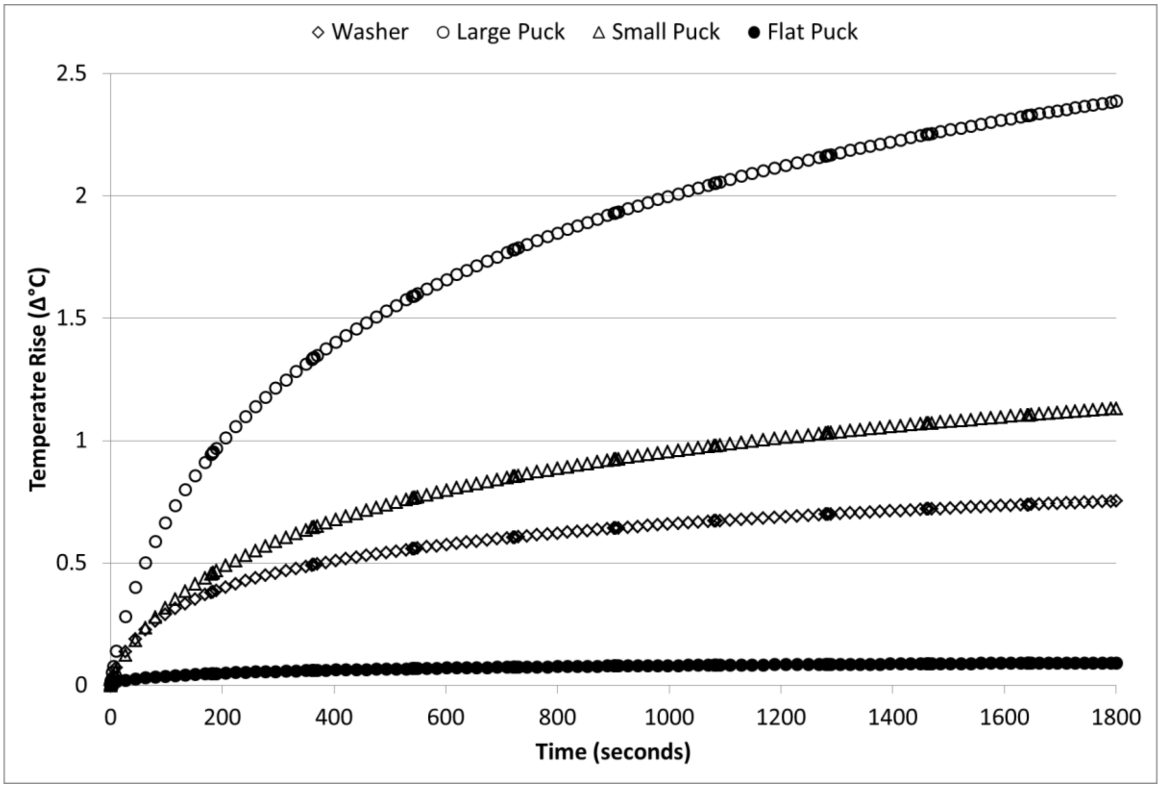

Figure 4.6 Simulated Temperature Rise (Δ°C) Results due to Gradient Heating at 25 T/s in Saline with Thermal Convection Coefficients of 5-20 W/m^2

From the figure, it can be seen that the Flat Puck had minimal heating, while the Small Puck climbed above 1°C, the Washer to 0.75°C and the Large Puck reached over 2°C temperature rise by the end of the 30 minutes (1800 seconds). Table 4.1 below lists the maximum temperature rise for each sample. This occurred at the final time step, 1800 seconds, for all of the samples. Note that the conductivity values for these simulations are available in Table 3.2.

Table 4.1 Maximum Simulation Temperature Rise (Δ°C) due to Gradient Heating at 25 T/s in Saline with Thermal Convection Coefficients of 5-20 W/m^2

Sample Name	**Maximum Temperature Rise (Δ°C)**
Large Puck	2.388
Small Puck	1.133
Flat Puck	0.093
Washer	0.754

4.2 Laboratory Experimentation and Validation

The graphical results from the infrared imaging test procedure in PAA detailed in Section 3.3.2.1 are included in Appendix A along with the equivalent graphics from the simulations. The maximum temperature probe testing results for the gradient induced heating in saline detailed in Section 3.3.2.2 are summarized in the following table for the four samples tested.

Table 4.2 Laboratory Results of Maximum Measured Temperature Rise (Δ°C) due to Gradient Heating at 25 T/s in Saline

Sample Name	**Channel 1: Top Edge**	**Channel 2: Top Middle**	**Channel 3: Bottom Middle**	**Channel 4: Bottom Edge**
Large Puck	1.81	1.57	1.59	2.07
Small Puck	0.86	0.91	0.91	1.53
Flat Puck	0.22	0.11	0.19	0.22
Washer	0.96	1.02	0.97	0.91

For each test sample, the channel with the highest temperature rise is plotted below over the entire scan duration. The absolute temperatures were converted to temperature rises by subtracting the starting temperature. For each sample, the 30 second moving average is plotted as a black line.

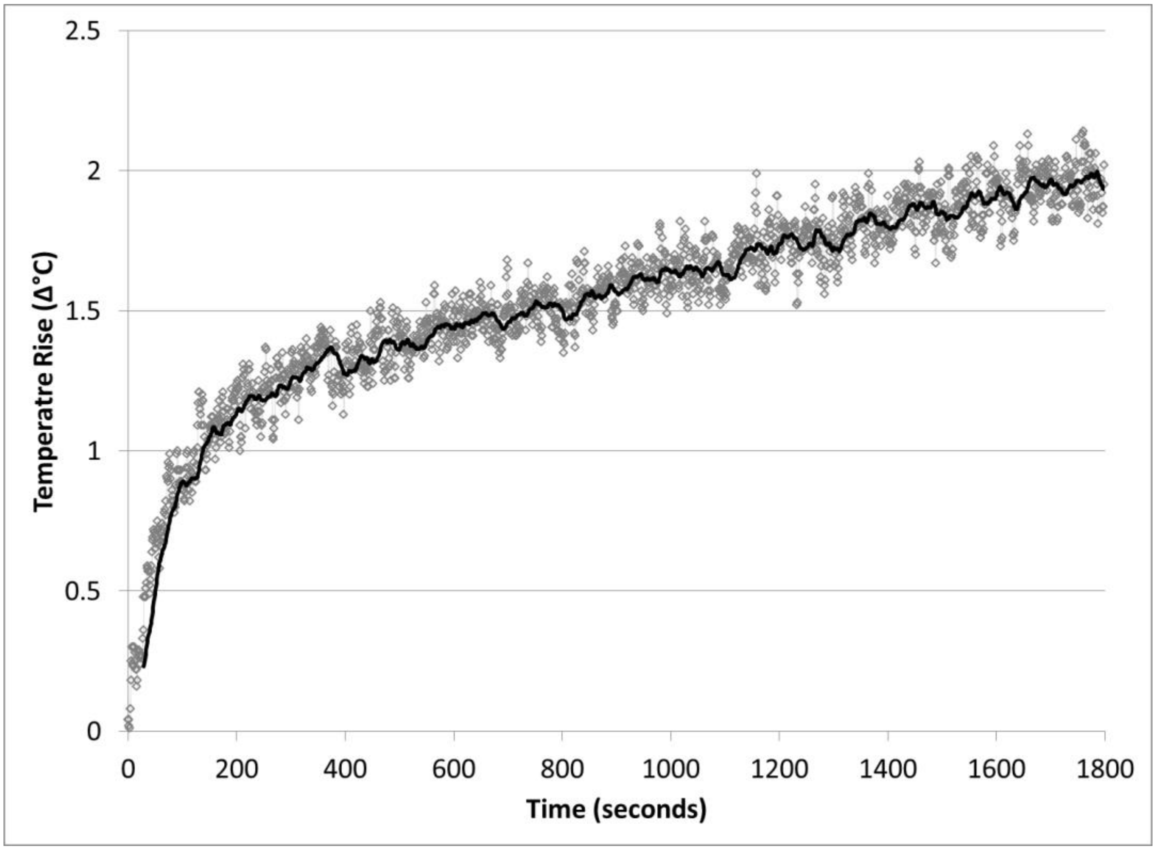

Figure 4.7 Temperature Rise versus Time for Channel 4 on Bottom Edge of Large Puck in Saline at Gradient dB/dT rms of 25 T/s

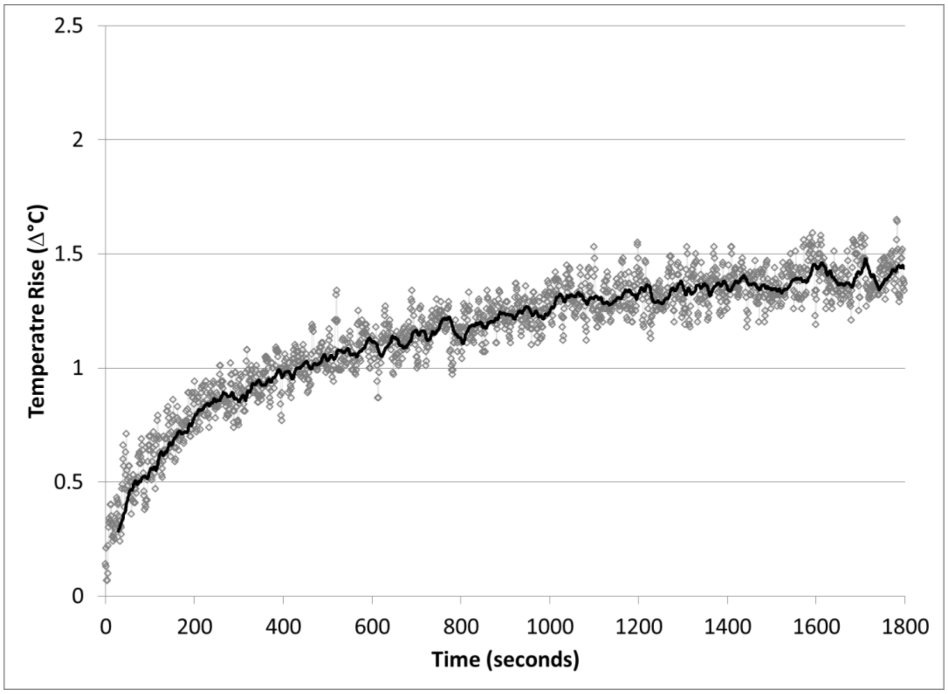

Figure 4.8 Temperature Rise versus Time for Channel 4 on Bottom Edge of Small Puck in Saline at Gradient dB/dT rms of 25 T/s

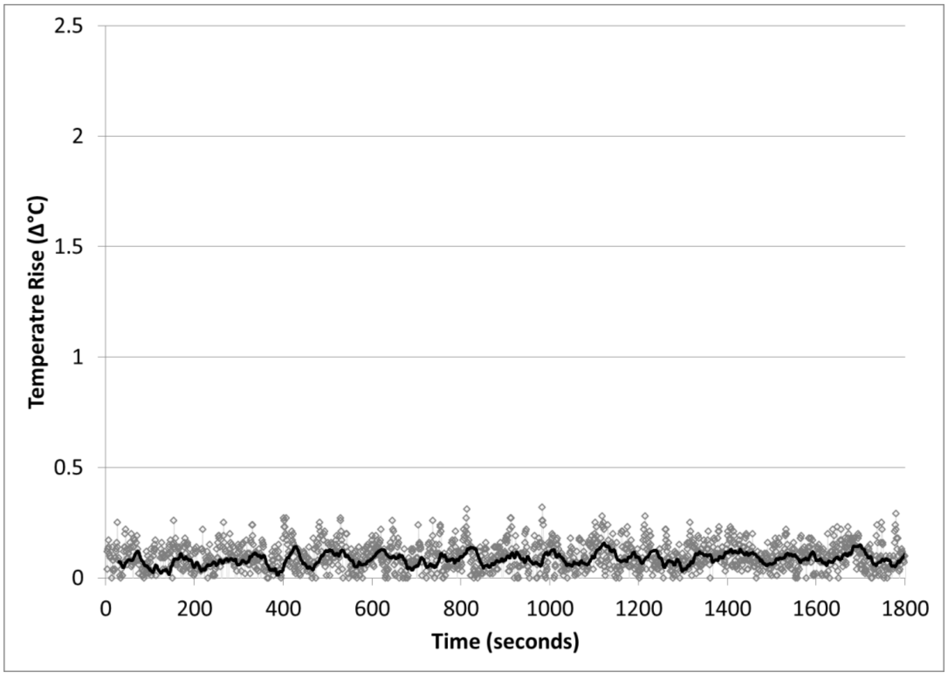

Figure 4.9 Temperature Rise versus Time for Channel 4 on Bottom Edge of Flat Puck in Saline at Gradient dB/dT rms of 25 T/s

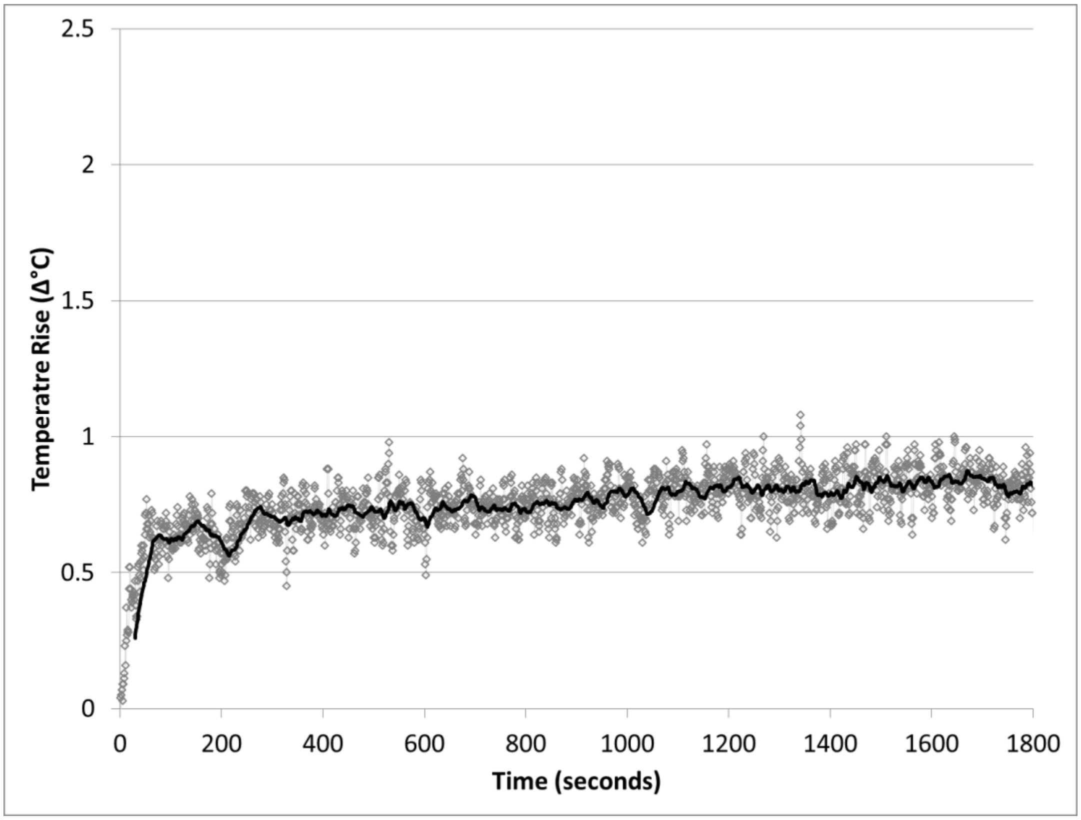

Figure 4.10 Temperature Rise versus Time for Channel 2 on Top Edge of Washer in Saline at Gradient dB/dT rms of 25 T/s

The scatter observed in the plots is a function of the Luxtron fiberoptic temperature probes. The moving average line helps show the general trend of the temperature rise over the 30 minute scan. For the other probes on each of the test sample, the curvature followed a similar pattern to the graphs shown.

4.3 Simulation Device Variations

Simulations were completed on the range of device variations listed in the test matrix of Figure 3.11. This allowed the impact of both diameter and thickness on device heating to be evaluated. Figure 4.11 shows the temperature rise as a function of device diameter. The three separate curves represent three different thickness values of the sample: 0.05cm, 0.6ccm and 1.27cm.

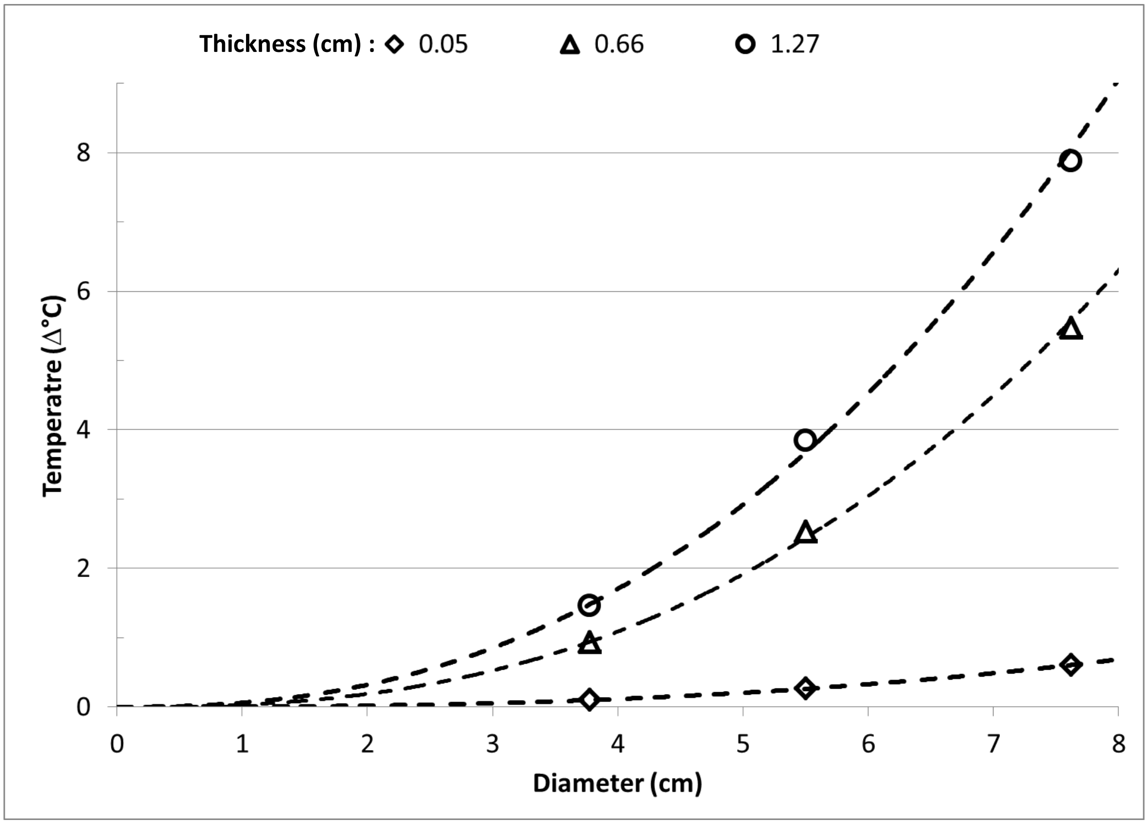

Figure 4.11 Simulated Temperature Rise versus Diameter for Titanium Disks at Gradient Strength of 25 T/s without Convection

The plotted curves in Figure 4.11 are power fits of the data points for each thickness. The equations for these three curves along with their respective coefficients of determination are listed below.

Thickness 1.27cm: $y = 0.0603x^{2.4107}\ R^2 = 0.9980$ (11)

Thickness 0.66cm: $y = 0.0325x^{2.5329}\ R^2 = 0.9989$ (12)

Thickness 0.05cm: $y = 0.0033x^{2.5741}\ R^2 = 0.9998$ (13)

In order to derive the curve fits, power equations were setup and the coefficients were solved. As expected, the power equation fits the curvature very well for each case. This is a result of the electric field being proportional to the radius of the device under test, which means that the maximum rise will scale with the square of the radius. This relationship can be derived by applying Stokes' Theorem to the Maxwell-Faraday equation presented in Equation 1, which results in the following equation:

$$\int E \cdot ds = -\frac{\partial \iint B \cdot dA}{\partial t} \tag{14}$$

Each side of the equation is then solved:

$$\int E \cdot ds = E * 2 * \pi * r \tag{15}$$

$$-\frac{\partial \iint B \cdot dA}{\partial t} = \left|\frac{\partial B}{\partial t}\right| * \pi * r^2 \tag{16}$$

Finally, the equations are set equal to each other and solved for *E*:

$$E * 2 * \pi * r = \left|\frac{\partial B}{\partial t}\right| * \pi * r^2 \tag{17}$$

$$E = \left|\frac{\partial B}{\partial t}\right| * \frac{r}{2} \tag{18}$$

For the thinnest sample, 0.05cm thick, the temperature does rise as a function of diameter, but at a significantly lower rate than the other thickness values. In order to evaluate the relationship between thickness and heating, the impact of device thickness on temperature is also shown in Figure 4.12. In this graph, the diameter is held constant at 3.78cm and the thickness is varied. The plotted line is a curved line fit; it is not an equation-based fit.

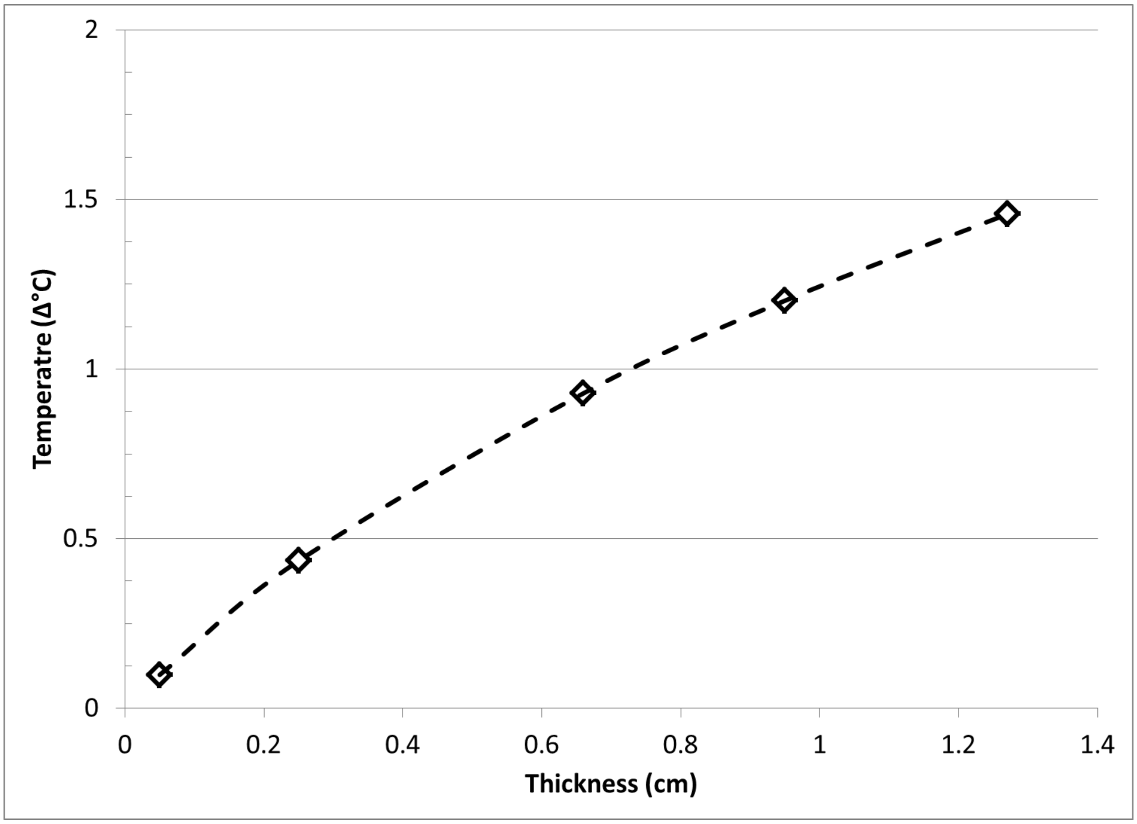

Figure 4.12 Simulated Temperature Rise versus Thickness for Titanium Disks with Diameter 3.78cm at Gradient Strength of 25 T/s without Convection

Figure 4.12 shows that increasing thickness has the direct result of increasing temperature rise. The relationship is not perfectly linear and could vary as a function of material and diameter. It would be expected that heating as a function of thickness would level off as the thickness approaches the electrical skin depth. The skin effect occurs because rapidly changing magnetic fields, such as the gradient magnetic field, do not completely penetrate the disk. The skin, or penetration, depth can be calculated from the following equation (Wansness, 1986):

$$\delta = \frac{1}{\sqrt{\pi * f * \mu * \sigma}} \tag{19}$$

Where δ is the skin depth in meters, f is the frequency in Hertz, σ is the electrical conductivity in siemens per meter (see Table 3.2) and μ is the magnetic permeability, which for non-ferromagnetic titanium is the permeability of free space ($4 * \pi * 10^{-7}$ H/m). When these values are enterred into Equation 19 for Grade 1 Titanium at 500Hz, the skin depth is 1.67cm. The curvature shown in Figure 4.12 appears to be leveling off at it approahces 1.4cm, but additional simulations are necessary to confirm the temperature at and beyond the skin depth. This is a potential area for future investigation.

CHAPTER 5. CONCLUSION

5.1 Discussion

When discussing the heating effects due to gradient MRI coils on an implantable medical device, there are two schools of thought. The first school of thought recognizes the physical possibility of an interaction, but believes the risk to the patient to be minimal, if none existent. The current literature, as discussed in Section 2.2, supports this theory with limited testing and analysis failing to demonstrate a significant patient risk due to the heating effects of gradient coils. The key here is that the current literature is limited in scope and quantity. The reasons for this include the very fact that the perceived risk is minimal and also because of the higher risks associated with the radiofrequency coils of the MRI scanner.

The second school of thought believes that the patient risk due to gradient induced heating is a real concern. This perspective is based on both the limitations of the current published evidence and the theoretical possibilities of heat given the vast range of implant sizes and compositions in the high energy field. The scope of this paper and research does not address this debate directly. It does, however, provide a tool and framework that will make the research and investigation much easier when answering the question of risk due to gradient induced heating of implantable devices.

The fact remains that the current regulatory landscape requires manufacturers of implantable medical devices to demonstrate safety, including the safety of the device with regards to gradient induced heating. Regardless of the actual risk, testing and evidence are still required to obtain MR Conditional labeling for products. Traditionally, this evidence is in the form of extensive in-vitro and in-vivo testing. This paper and research supports computer simulation as another tool for equally effective analysis of gradient induced heating on implantable devices.

The heating effects due to gradient MRI coils on implantable devices have been successfully modeled using ANSYS Maxwell and ANSYS Mechanical. The success of these simulations comes from their comparison to physical testing of comparable samples. This comparison is made by matching the maximum simulated results from Table 4.1 to the maximum measured temperatures from Table 4.2, which is shown in the table below.

Table 5.1 Measured versus Simulated Temperature Rise (Δ°C) Results due to MRI Gradient induced Heating at 25 T/s in Saline

Sample Name	**Maximum Simulated Temperature Rise (Δ°C)**	**Maximum Measured Temperature Rise (Δ°C)**
Large Puck	2.388	2.07
Small Puck	1.133	1.53
Flat Puck	0.093	0.22
Washer	0.754	1.02

When comparing the simulated results to the measured results, it is important to note two key limitations of the physical testing. First, even though the hotspots for each sample were identified using thermal imaging, shown in Appendix A, the maximum temperature location may not have been measured. This is highlighted when comparing the temperature measurements from different surfaces of the devices and also the variation between the middle and the edge of the samples. The surfaces of the devices were exposed to equivalent fields since the devices were placed in the center of the test environment. The differences in measured temperature between the two surfaces of each device indicate testing variability. The variability in temperature along the surface is also demonstrated by the measured differences between the middle and the edge of the test samples.

The second limitation of the physical testing is the Luxtron fiberoptic temperature probes used. These probes were used because their measurements are not impacted by the gradient field. The tradeoff is that the probes have a limited accuracy and will oscillate when measuring temperature, which can be seen in Figure 4.7, Figure 4.8, Figure 4.9, and Figure 4.10. This oscillation limits the accuracy of the probes to approximately 0.5°C. Even the moving 30 second averages displayed as the black line on the figures shows significant oscillation.

Given the limitations of the measurement system, the Large Puck, Small Puck, Flat Puck, and Washer all have good matches between the simulated results and the measured results. These samples represent a range of thickness, radii, geometry, and even material. The Large Puck was grade 5 titanium, the Small Puck and Flat Puck were both grade 1 titanium, and the Washer was stainless steel. The Large Puck was simulated as both grade 5 and grade 1 titanium, with the Grade 5 temperature rise in Table 4.1 of 2.388°C and the grade 1 temperature rise in Figure 4.11 of 7.872°C. This difference in the simulated results is consistent with the expected variation due to the differences between the material properties of the two grades of titanium.

Differences between the measured data and simulated data could also exist due to a limitation in the computer simulation. A variation exists between the simulation results and the measured results in the curvature of the heating profile, as seen when comparing Figure 4.6 to Figure 4.7 and Figure 4.10. The measured graphs appear to have a larger initial temperature rise compared to the simulated results. This could indicate a physical phenomenon that the simulation is not capturing. Possibilities include modeling the external components of the test environment and also gradient coil properties not included in the model. This is a continued area of research and the next step in improving the validation of the computer simulation setup.

Following the validation exercise, the computer simulation setup was then used to understand the impact of implant radius and thickness on device heating. The impact of radius, or diameter, on heating is shown in Figure 4.11. In this figure, three separate curves are shown for three different thickness values. All of the simulations were conducted on Grade 1 Titanium without convection. The graph shows the combined effect of both thickness and radius. The impact of radius alone appears to follow a power equation fit, as expected since the induced electric field scales with radius. For extremely small thickness values, such as the 0.05cm models, even though the thickness impacts heating, the temperature rise values stay well below critical thresholds. However, for thicker metals, the temperature rise increases far more quickly as a function of diameter.

The impact of thickness is shown in Figure 4.12 for a constant diameter range of models. These simulations were also conducted on Grade 1 Titanium samples without convection. While smaller thickness samples do not show large temperature rises, the temperature does increase at a fairly constant rate as a function of thickness. In the example shown, the temperature appears to level off as it approaches the skin depth of the sample. This is important to keep in mind, especially when considering design and manufacturing tradeoffs of implantable medical devices. Future simulations could extend this curve while also generating similar curves for other materials in additional exposure environments.

While the simulation experiments on the variables discussed above are interesting, they are barely the tip of the iceberg of potential parameters and effects that could be characterized and understood with a successful computer simulation of the gradient induced heating on implantable medical devices. It is important to highlight that heating can occur not only on the external surface, or case, of the implantable device, but also any large metallic surface inside of a device. For example, the battery of a none-rechargeable implantable neurostimulator can be quite large and would be more likely to have a thicker metal than the external case. In this scenario, the external case may show minimal heating by itself, but the battery could heat up extensively and transfer that heat to the external case and onto the patient. A limited computer simulation of just the external case would fail to show this effect.

The simulations completed for this work contribute to the discussion of parameter characterization, but are just the first step. The real success lies in the potential of computer simulation to answer questions that would have been very difficult, time consuming and expensive to fully answer with physical testing. Even though the success of the computer simulation model as measured in accuracy relative to the laboratory test results is encouraging, a number of areas still exist for future exploration that are detailed in the next section.

To summarize, the interaction between implantable medical devices and MRI environments is complex. A key component of this interaction is the induced heating that is possible due to eddy currents created on metal objects from the MRI gradient coils. This heating is a potential patient risk that limits the eligibility of patients to receive an MRI. For patients with implantable medical devices, the ability to safely undergo MRI scanning is critical to ensuring the highest standard of care. Even though current literature fails to demonstrate significant heating due to gradient coils, it is limited in scope and quantity. Also, the current regulatory landscape requires extensive safety testing that is often expensive and time consuming. While the complicated question of heating potential remains open, computer simulation is now a proven tool that can provide easier and more thorough analysis for future evaluations.

5.2 Future Work

As mentioned in the previous section, this research opens up an extensive collection of potential future work. The ultimate goal would be to improve the accuracy of the simulation and also expand the scope of the investigation to help characterize the interaction and provide clarity when determining the safety of implantable medical devices. The future work falls into two main categories: model improvements and additional simulations.

For model improvements, in addition to addressing the sources of variation discussed in the previous section, updates can be made not only to the detail of the actual model but also to the physical properties inputted into the model. One particular example is the material properties of the samples, which were determined by literature values but ideally would be characterized through independent testing. This has the potential to significantly improve the accuracy of the model. Another example is the convection coefficients used in the saline simulations. The coefficient was estimated based on equations but ideally would be independently calculated for each sample in the actual test medium using laboratory testing.

As for the detail of the model, a point of interest for actual implantable medical devices, versus metal disks, would be the battery within the device and how energy is coupled between the battery and the external case. This could be a major driver of observed heating due to gradient coils and a potential design source for risk mitigation. The computer simulations could also be used to characterize the effects of battery heating outside of an MRI environment.

Another potential source for future work would be an expansion of simulation conditions. Especially after the model improvements discussed above, the simulations could be used to study a range of parameters beyond radius and thickness. This could include different materials and geometries for implantable devices along with different orientations within the gradient environment and eventually complex interactions that are a function of multiple variables. The list is far too extensive to detail here but would begin to characterize the broad landscape of potential interactions highlighting the critical ones to support MRI safety assessments and design choices for a range of implantable medical devices.

REFERENCES

REFERENCES

ACR. (2013). *Appropriateness Criteria.* American College of Radiology.

ASTM F2052-06e1. (2006). Standard Test Method for Measurement of Magnetically Induced Displacement Force on Medical Devices in the Magnetic Resonance Environment. West Conshohocken, PA: ASTM International. doi:10.1520/F2052-06E01

ASTM F2213-06. (2011). Standard Test Method for Measurement of Magnetically Induced Torque on Medical Devices in the Magnetic Resonance Environment. West Conshohocken, PA: ASTM International. doi:10.1520/F2213-06R11

ASTM Standard F2182-11a. (2011). Standard Test Method for Measurement of Radio Frequency Induced Heating On or Near Passive Implants During Magnetic Resonance Imaging. West Conshohocken, PA: ASTM International. doi:10.1520/F2182-11A

Buchli, R., Boesiger, P., & Meier, D. (1988, July). Heating effects of metallic implants by MRI examinations. *Magnetic Resonance in Medicine, 7*(3), 255-261.

Butala, N. B., Shehada, R. E., Constandi, P. N., Dianaty, A., & Jurkowski, K. (2011). Maximum dB/dt and Switching Noise in 1.5T MRI Scanners for Safety Evaluation of Active Implantable Medical Device. International Society for Magnetic Resonance in Medicine. Retrieved from http://cds.ismrm.org/protected/11MProceedings/files/1788.pdf]

Clare, S. (2006, December 14). *Functional MRI: Methods and Applications*. Retrieved 2013, from The University of Nottingham: http://users.fmrib.ox.ac.uk/~stuart/thesis/index.html

Coyne, K. (n.d.). *MRI: A Guided Tour*. Retrieved 2013, from National High Magnetic Field Laboratory: http://www.magnet.fsu.edu/education/tutorials/magnetacademy/mri/fullarticle.html

FDA. (2013, June 24). *March 2013 PMA Approvals*. Retrieved March 7, 2014, from U.S. Food and Drug Administration: http://www.fda.gov/MedicalDevices/ProductsandMedicalProcedures/DeviceApprovalsandClearances/PMAApprovals/ucm353945.htm

Finelli, D. A., Nyenhuis, J. A., & Gonzalez-Martinez, J. (2002). MR Imaging-Related Heating of Deep Brain Stimulation Electrodes: In Vitro Study. *American Journal of Neuroradiology*(23), 1795-18002.

Foreman, C. (2011, February 8). *P090013 Revo MRI SureScan Pacing System.* Retrieved March 7, 2014, from U.S. Food and Drug Administration: http://www.accessdata.fda.gov/cdrh_docs/pdf9/p090013a.pdf

Gonzalez, B. d. (2009). Project Cancer Risks From Computed Tomographcic Scans Performed in the United States in 2007. *Arch Intern Med*.

Hornak, J. P. (n.d.). *The Basics of MRI*. Retrieved January 2014, from Chester F. Carlson Center for Imaging Science: http://www.cis.rit.edu/htbooks/mri/index.html

IMV. (2012). *Benchmark Report MR.* Des Plaines: IMV Medical Information Division, Inc.

ISO/TS 10974. (2012). Assessment of the safety of magnetic resonance imaging for patients with an active implantable medical device. International Organization for Standardization.

Lee, H.-H. (2012). *Finite Element Simulations with ANSYS Workbench 14 Theory, Applications, Case Studies.* SDC Publications.

Mohsin, S. A., Nyenhuis, J., & Masood, R. (2010). Interaction of Medical Implants with the MRI Electromagnetic Fields. *Progress In Electromagnetics Research C, 13*, 195-202.

Nyenhuis, J. A., Park, S.-M., Kamondetdacha, R., Amjad, A., Shellock, F., & Rezai, A. (2005, September). MRI and implanted medical devices: basic interactions with an emphasis on heating. *Device and Materials Reliability, IEEE Transactions on, 5*(3), 467 - 480.

Sanchez, C. C. (2008). *Forward and inverse analysis of electromagnetic fields for MRI using computational techniques.* The University of Nottingham.

Schaefer, D. J., Bourland, J. D., & Nyenhuis, J. A. (2000). Review of Patient Safety in Time-Varying Gradient Fields. *Journal of Magnetic Resonance Imaging*(12), 20-29.

Schueler, B. A., Hammer, B. E., & Kucharczyk, J. (1999). MRI Compatibility and Visibility Assessment of Implantable Medical Devices. *Journal of Magnetic Resonance Imaging*(9), 596-603.

Smelka, R., Armao, D., Elias, J., & Huda, W. (2007). Imaging Strategies to Reduce the Risk of Radiation in CT Studies, Including Selectice Substitution with MRI. *J Magnet Res Imag*(25), 900-909.

Tipler, P. A., & Mosca, G. (2008). *Physics for Scientists and Engineers* (Sixth ed.). New York, NY: W. H. Freeman and Company.

Wansness, R. K. (1986). *Electromagnetic Fields* (2nd ed.). Hoboken, NJ: John Wiley & Wiley Sons, Inc.

Wilkoff, B., Bello, D., taborsky, M., Vymazal, J., Kanal, E., Heurer, H., . . . Sommer, T. (2011, January 8). Magnetic resonance imaging in patients with a pacemaker system designed for the magnetic resonance environment. *Heart Rhythm, 8*(1), 65-73.

Woods, T. O. (2008). *Establishing Safety and Compatibility of Passive Implants in the Magnetic Resonance (MR) Environment.* Rockville: U.S. Department of Health and Human Resources, Food and Drug Administration, Center for Devices and Radiological Health.

APPENDIX

APPENDIX GRADIENT HEATING OF DEVICE VISUAL DISTRIBUTION

Results from the infrared imaging test procedure detailed in Section 3.3.2.1 are shown in the following figures for the Large Puck and Small Puck. The images show the heat distribution along the surface of the sample tested. Note that the resolution and clarity is affected by the fact that the image is being taken through a thin layer of gelled saline (or PAA) on top of the sample.

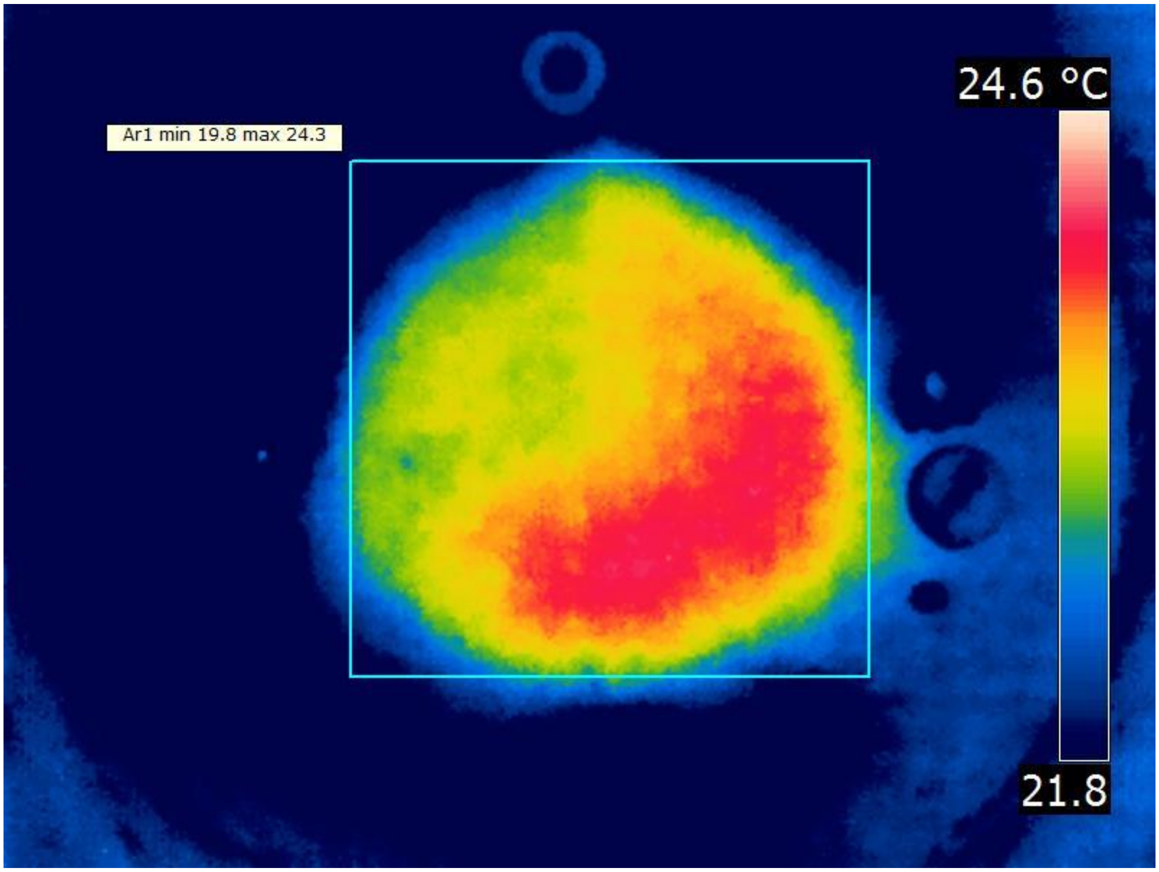

Figure A 1 Infrared Image of Large Puck in Gradient MRI Field

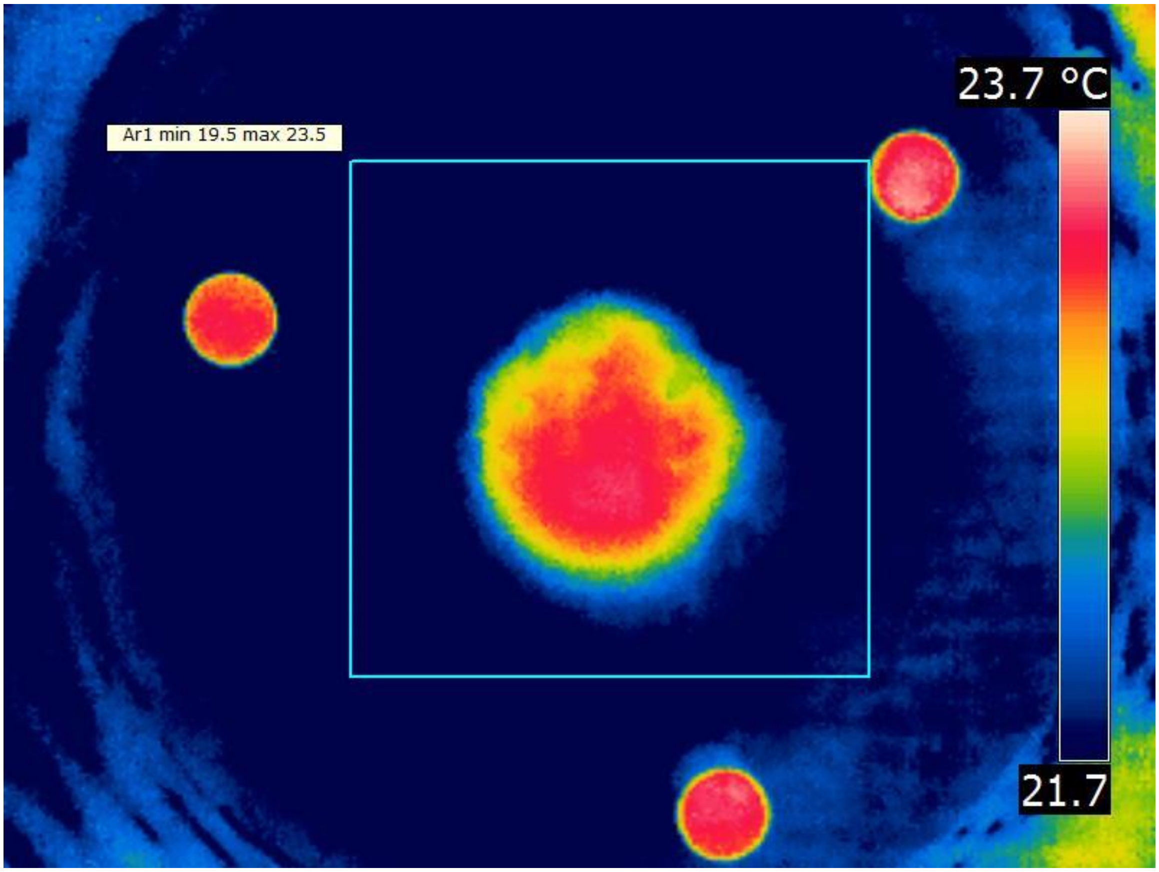

Figure A 2 Infrared Image of Small Puck in Gradient MRI Field

The heating profiles in the images above can be compared to the heating profiles generated by the computer simulation. Graphics of the transient thermal solutions for the four samples both physically tested and modeled are shown below without convection. The graphics show the heating profile across the surface at the final time step (1800 seconds).

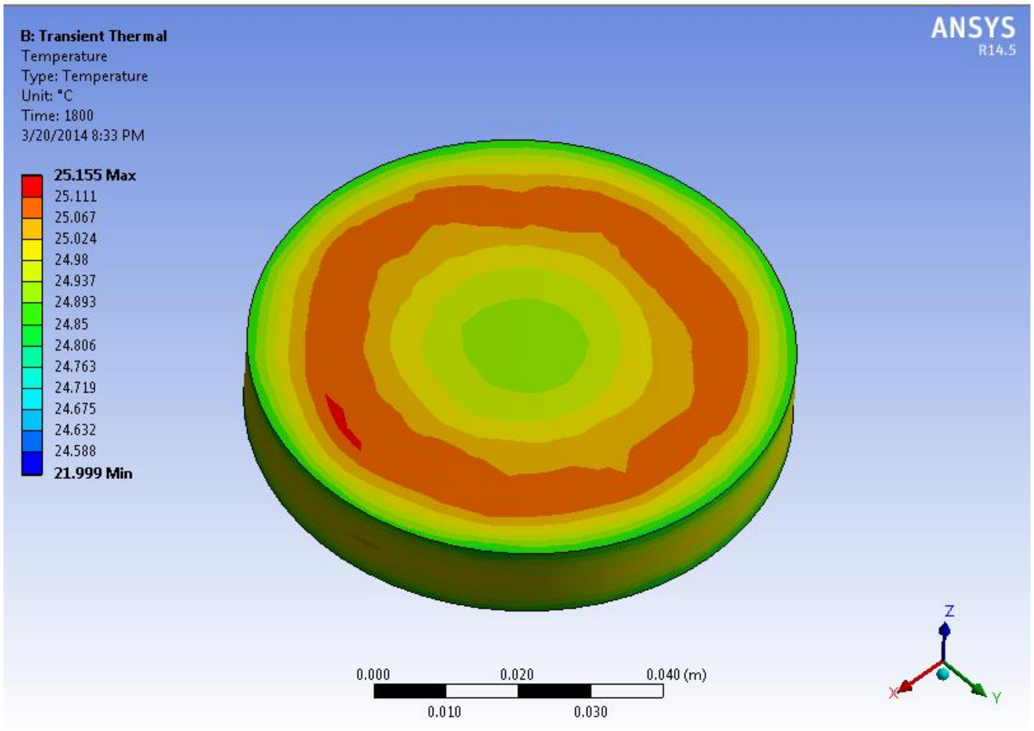

Figure A 3 Transient Thermal Solution for Large Puck

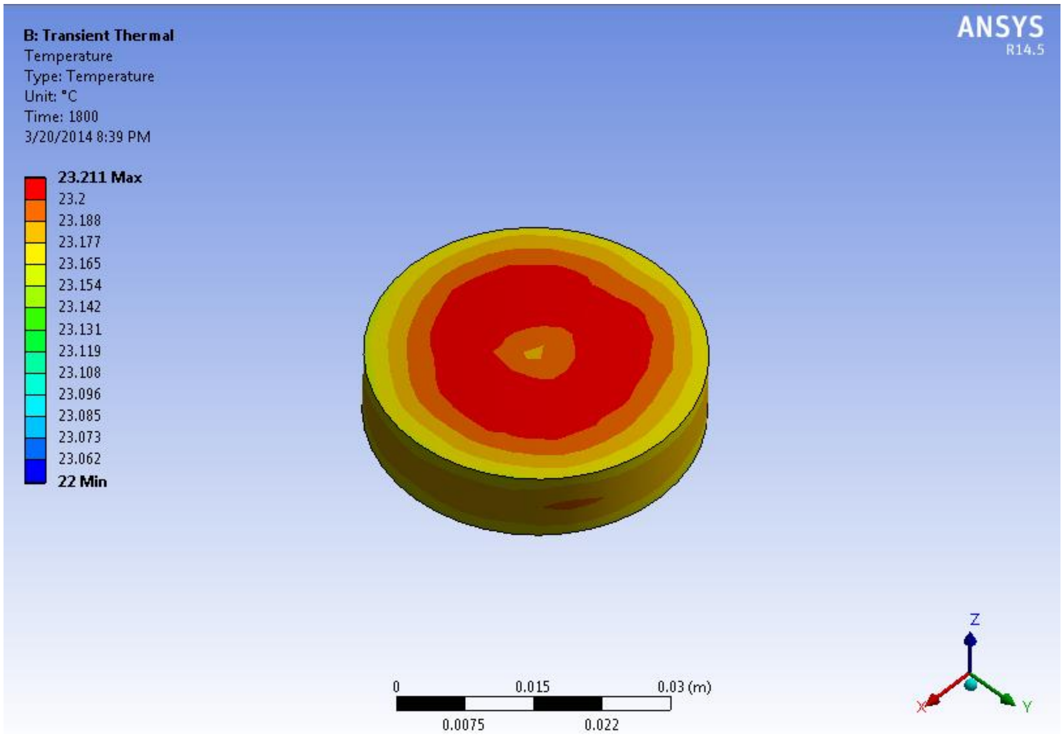

Figure A 4 Transient Thermal Solution for Small Puck

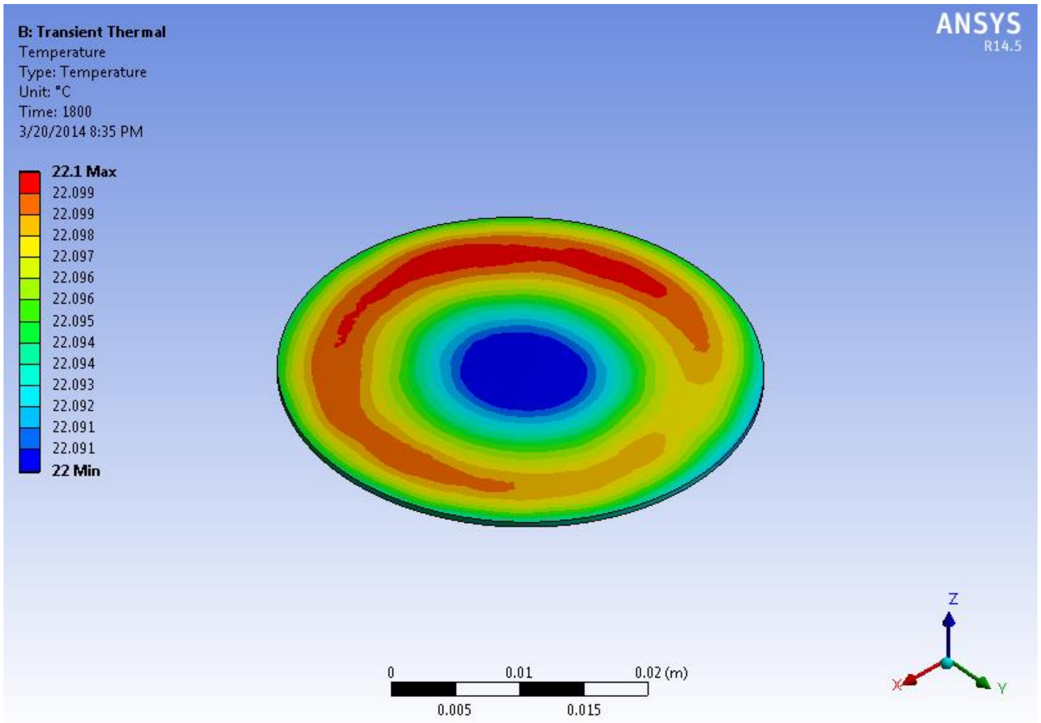

Figure A 5 Transient Thermal Solution for Flat Puck

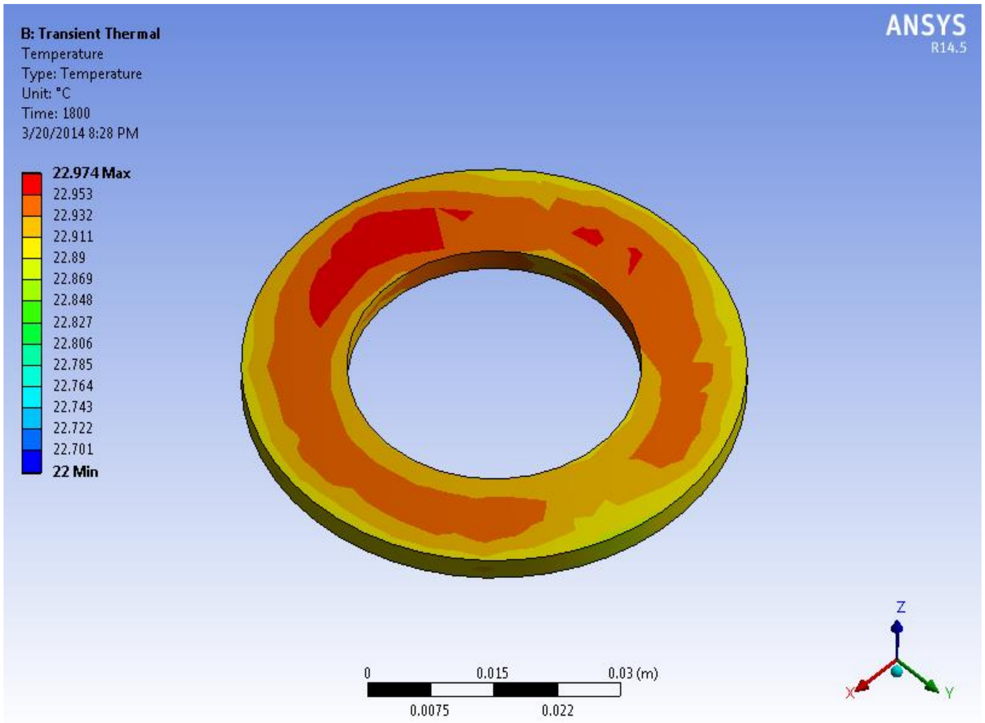

Figure A 6 Transient Thermal Solution for Washer

Finally, a cross section of the simulation test environment was taken at the final time step for one of the titanium samples to show the heat distribution around the sample and the surrounding environment. This is shown in the figure below.

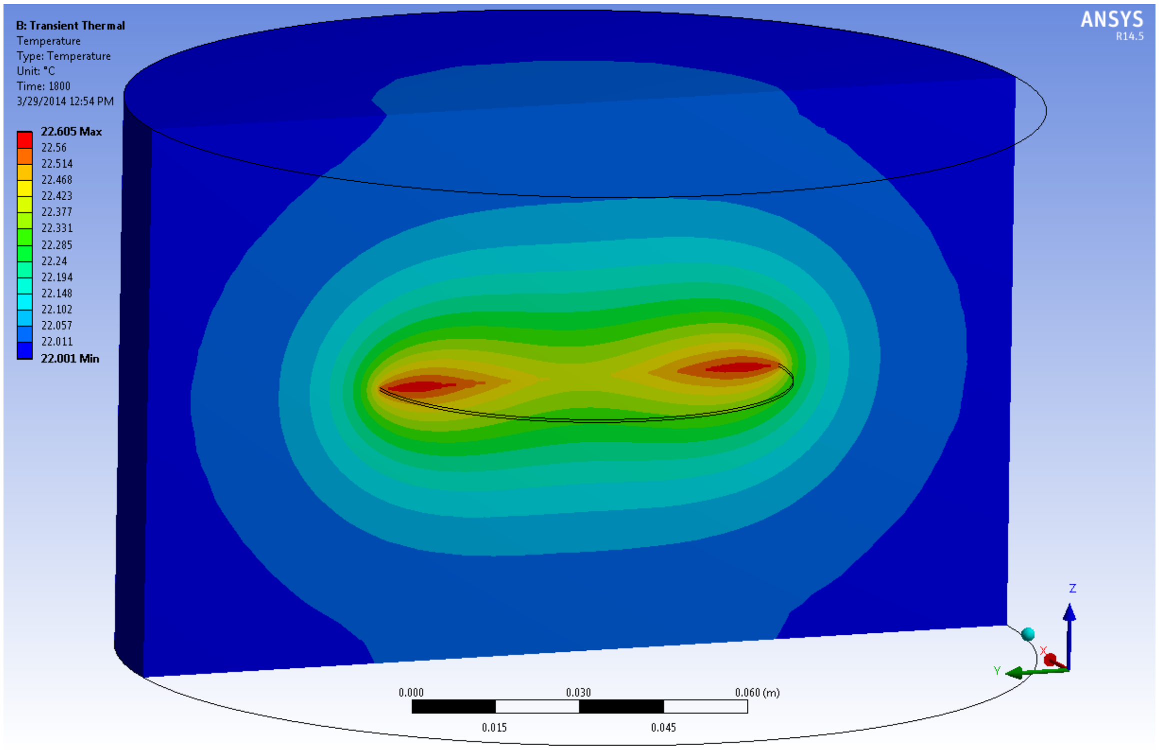

Figure A 7 Transient Thermal Solution for Titanium Sample with Environment

VITA

VITA

Bryan Stem
Graduate School, Purdue University

Education

B.S.E., Mechanical Engineering, 2009, Duke University, Durham, North Carolina

Professional Experience

Senior Mechanical Design Engineer, 2009-current, Medtronic, Minneapolis, Minnesota
DRM (Six Sigma) Black Belt, 2013-current, Medtronic, Minneapolis, Minnesota

Research Interests

The primary area of research interest and expertise is the safety of implantable medical devices in an MRI environment. In particular, radiofrequency and gradient induced heating and methods for evaluating safety. Another broader research interest is the product development and research of implantable medical devices. An area of focus within product development is the use of statistical and quality tools to improve processes and products, such as Six Sigma methodology.